Bioactive Materials 6 (2021) 2315–2330

Contents lists available at ScienceDirect

Bioactive Materials

journal homepage: www.sciencedirect.com/journal/bioactive-materials

Regulation of extracellular bioactive cations in bone tissue microenvironment induces favorable osteoimmune conditions to accelerate *in situ* bone regeneration

Zhengjie Lin [a,b,j,*], Danni Shen [c,d], Weixiao Zhou [e], Yufeng Zheng [c], Tiantian Kong [e], Xuanyong Liu [f], Shuilin Wu [g], Paul K. Chu [h], Ying Zhao [i], Jun Wu [d], Kenneth M.C. Cheung [b], Kelvin W.K. Yeung [b,d,**]

[a] College of Chemistry and Environmental Engineering, Shenzhen University, Shenzhen, 518060, China
[b] Department of Orthopaedics and Traumatology, The University of Hong Kong, Hong Kong, China
[c] Department of Materials Science and Engineering, College of Engineering, Peking University, Beijing, 100871, China
[d] Shenzhen Key Laboratory for Innovative Technology in Orthopaedic Trauma, The University of Hong Kong Shenzhen Hospital, 1 Haiyuan 1st Road, Futian District, Shenzhen, China
[e] Guangdong Key Laboratory for Biomedical Measurements and Ultrasound Imaging, Department of Biomedical Engineering, School of Medicine, Shenzhen University, Shenzhen, 518060, China
[f] State Key Laboratory of High Performance Ceramics and Superfine Microstructure, Shanghai Institute of Ceramics, Chinese Academy of Sciences, Shanghai, 200050, China
[g] School of Materials Science & Engineering, the Key Laboratory of Advanced Ceramics and Machining Technology by the Ministry of Education of China, Tianjin University, Tianjin, 300072, China
[h] Department of Physics, Department of Materials Science and Engineering, City University of Hong Kong, Tat Chee Avenue, Kowloon, Hong Kong, China
[i] Centre for Human Tissues and Organs Degeneration, Shenzhen Institutes of Advanced Technology, Chinese Academy of Sciences, Shenzhen, 518055, China
[j] State Key Laboratory of Bioelectronics, School of Biological Science and Medical Engineering, Southeast University, Nanjing, 210096, China

ARTICLE INFO

Keywords:
Bone regeneration
Osteoimmunomodulatory property
Osteoimmune environment
Macrophage polarization
Magnesium ions

ABSTRACT

The design of orthopedic biomaterials has gradually shifted from "immune-friendly" to "immunomodulatory," in which the biomaterials are able to modulate the inflammatory response via macrophage polarization in a local immune microenvironment that favors osteogenesis and implant-to-bone osseointegration. Despite the well-known effects of bioactive metallic ions on osteogenesis, how extracellular metallic ions manipulate immune cells in bone tissue microenvironments toward osteogenesis and subsequent bone formation has rarely been studied. Herein, we investigate the osteoimmunomodulatory effect of an extracellular bioactive cation (Mg^{2+}) in the bone tissue microenvironment using custom-made poly lactic-co-glycolic acid (PLGA)/MgO-alendronate microspheres that endow controllable release of magnesium ions. The results suggest that the Mg^{2+}-controlled tissue microenvironment can effectively induce macrophage polarization from the M0 to M2 phenotype via the enhancement of anti-inflammatory (IL-10) and pro-osteogenic (BMP-2 and TGF-β1) cytokines production. It also generates a favorable osteoimmune microenvironment that facilitates the proliferation and osteogenic differentiation of bone marrow mesenchymal stem cells. The *in vivo* results further verify that a large amount of bony tissue, with comparable bone mineral density and mechanical properties, has been generated at an early post-surgical stage in rat intramedullary bone defect models. This study demonstrates that the concept of *in situ* immunomodulated osteogenesis can be realized in a controlled magnesium tissue microenvironment.

Peer review under responsibility of KeAi Communications Co., Ltd.
* Corresponding author. College of Chemistry and Environmental Engineering, Shenzhen University, China.
** Corresponding author. Department of Orthopaedics and Traumatology, The University of Hong Kong, Hong Kong, China.
E-mail addresses: linzhengjie1218@163.com, linzj@szu.edu.cn (Z. Lin), wkkyeung@hku.hk (K.W.K. Yeung).

https://doi.org/10.1016/j.bioactmat.2021.01.018
Received 17 November 2020; Received in revised form 14 January 2021; Accepted 16 January 2021
Available online 23 January 2021

1. Introduction

In clinical practice, most orthopedic diseases, such as osteoma resection, revision surgery, high energy trauma, developmental deformities, and bone infection, lead to significant bone loss [1]. Furthermore, bone regeneration procedures are in high demand due to the aging population. Although various choices are available, the critical-sized bone defects treatment, in particular, remains challenging [2]. The trend has shifted towards biomaterials-mediated osteogenesis in recent years, enabling the direct modulation of osteogenesis and/or angiogenesis of stem cells to the osteoblastic lineage for bone regeneration [3]. When biomaterials are implanted into the human body, immune cells are actively recruited to the biomaterials, which triggers a host inflammatory response and local tissue inflammation [4–6]. In brief, monocytes in the host immune system adhere to the implanted biomaterial surface and differentiate into M1/M2 macrophages. The cytokines secreted by macrophages recruit other immune cells that initiate a foreign body reaction, inflammatory modulation, and subsequent bone healing. Advances in bone tissue engineering have led to a consensus that the physiochemical features of biomaterials can also trigger an inflammatory reaction at the implantation site, giving rise to positive or negative effects on bone regeneration [7]. Therefore, the development of biomaterials as bone substitutes should not only focus on direct osteogenesis regulation but also emphasize the local inflammatory response that will lead to a favorable osteoimmune tissue microenvironment. Indeed, immune cells are actively involved in bone remodeling and resorption since the cells in the immune and musculoskeletal systems share common signaling molecules, receptors, and cytokines, such as interleukin-6 (IL-6) and tumor necrosis factor-α (TNF-α) [8]. Among all the immune cells, macrophages have attracted much attention as the paramount effector cells that regulate the inflammatory response in addition to the plasticity feature upon of cellular polarization [9]. The literature highlights that the surface topography, material stiffness, porosity, and chemical cues of biomaterials can direct M1/M2 macrophage polarization [10,11]. M1 macrophages express high levels of IL-6, TNF-α, and IL-1β pro-inflammatory cytokines, thereby promoting undesirable inflammatory responses in the tissue microenvironment [12]. In contrast, M2 macrophages secrete anti-inflammatory cytokines, mainly IL-10, IL-13, IL-4, and arginase-1 (Arg 1), that contribute to osteogenesis and angiogenesis during the bone healing process via the release of vascular endothelial growth factor (VEGF) by endothelial cells or bone morphogenetic protein-2 (BMP-2) by mesenchymal stem cells [13]. Given the superior plasticity of macrophages (M1/M2 phenotype switch), a new pathway may be developed, allowing osteoimmunomodulatory biomaterials to modulate macrophages to secrete osteogenic cytokines in order to induce a favorable local osteoimmune microenvironment for bone regeneration.

Recently, the release of bioactive ions with specific concentrations *in vivo* (e.g., silicon, copper, strontium, magnesium, calcium, cobalt, and zinc) seems to be a cost-effective approach to stimulate bone regeneration [14–17]. Magnesium, an abundant trace element in bone tissue, is essential for the formation of biological apatite, enzymes, proteins, and nucleic acids and plays a vital role in the bone mineralization process and immune system [18]. Furthermore, magnesium ions trigger the differentiation of mesenchymal stem cells to chondrocytes by suppressing activated macrophage-induced inflammation [19,20]. Additionally, magnesium ions can also inhibit osteoclastogenesis by down-regulating the pro-inflammatory cytokines and modulate the bone tissue microenvironment to recruit osteogenic cells for bone regeneration [21]. However, high doses of magnesium ions in the local tissue microenvironment jeopardize osteogenic differentiation and bone mineralization, leading to osteomalacia-associated diseases [22,23]. Consequently, we hypothesize that manipulating magnesium ions in the local microenvironment can generate a robust osteoimmune microenvironment for bone regeneration. Nevertheless, little is known about how extracellular magnesium ions modulate the local bone microenvironment to osteoimmune-favored conditions that lead to subsequent bone regeneration.

In order to investigate the osteoimmunomodulatory effect of extracellular magnesium ions on the osteoimmune environment, we designed a PLGA/MgO-alendronate microsphere system comprising of lactic-co-glycolic acid (PLGA), magnesium oxide (MgO) nanoparticles, and alendronate. This customized magnesium ion delivery system possesses bone affinity properties and enables the controlled delivery of magnesium ions into the bone tissue microenvironment. As illustrated in Scheme 1a, we cultured macrophages on a PLGA/MgO-alendronate microsphere to investigate the osteoimmunomodulatory effects of controllable magnesium-ion delivery on macrophage inflammatory responses and the osteogenic activity of BMSCs in a macrophage-conditioned medium. Finally, a mouse air pouch model and a rat intramedullary bone defect model were employed to evaluate *in vivo* immunomodulatory responses and bone repair. The present study demonstrates the osteoimmunomodulatory functions of the PLGA/MgO-alendronate microsphere for further applications in bone regeneration.

2. Materials and methods

2.1. Synthesis of PLGA/MgO-alendronate microsphere

PLGA (75:25, carboxylic acid terminated, Mw = 25000–48000, Aldrich) and magnesium oxide (MgO) nanoparticles (PDF3973; Wako, Japan) were utilized in this experiment, while sodium alendronate powder (Wako, Japan) was used to modify the PLGA polymer for bone affinity property. As described in previous work [24], MgO nanoparticles were modified by 3-(Trimethoxysilyl)propyl methacrylate (TMSPM, Sigma, USA). All other reagents were used as an analytical grade.

Prior to the electrospinning fabrication, the PLGA-alendronate conjugate was prepared by the reaction method in the water phase [25,26]. Specifically, sodium alendronate powder (0.25 M) was dissolved in 8% aqueous acetic acid, followed by lyophilization for 48 h. The PLGA polymer was dissolved in the 2-morpholinoethanesulfonic (MES, pH 5.5) for 4 h, and the carboxylic groups of PLGA were activated by the addition of 100 mg 1-ethyl-3(3-dimethylaminopropyl)carbodiimide hydrochloride (EDC), 60 mg N-hydroxy-succinimide (NHS), and 8 mg ethylenediamine under magnetic stirring overnight at ambient temperature. The activated by-product was filtered with a pore size of 0.22 μm. Subsequently, cold diethyl ether was utilized to precipitate the NHS-activated PLGA, and 5 mg lyophilized alendronate with activated PLGA was added into a 20 ml mixture solution of 19 ml dimethylsulfoxide (DMSO) and 1 ml deionized (DI) water under magnetic stirring for 36 h. The PLGA-alendronate conjugate was deposited in cold diethyl ether and DI water, respectively. Finally, the as-fabricated conjugate was lyophilized for 48 h.

The microfluidic electrospraying system is composed of a high voltage power source (Dongxing Technical, Ltd. Co, China), a high-precision syringe pump (LSP01-2A, Longer Pump Inc., China) with controllable flow rate, customized concentric stainless steel nozzles (inner diameter and outer diameter: 0.55/0.88 mm, Dongxing Technical, Ltd. Co, China) and a collector. Briefly, the PLGA-alendronate conjugate (7% w/v) was prepared in the dichloromethane (DCM) solution, and MgO nanoparticles were suspended into the PLGA solution. The initial weight feeding ratio of PLGA/MgO was 1:0.2 (w:w), and the mixed solution was loaded into a 5 ml syringe. Following this, the syringe was placed on the pump to precisely control the flow rate while the solution was fed via a silicone tube into the nozzle. Under the electric field, a jet was formed at the nozzle tip by modulating the voltage. Microspheres were prepared by rapid solvent evaporation and then collected in the aluminum foil. During the fabrication process, the applied flow rate, voltage, and collection distance were optimized at 500 μl/h, 15 kV, and 22 cm, respectively. After collection, PLGA/MgO-alendronate microspheres were lyophilized for 72 h. The PLGA and

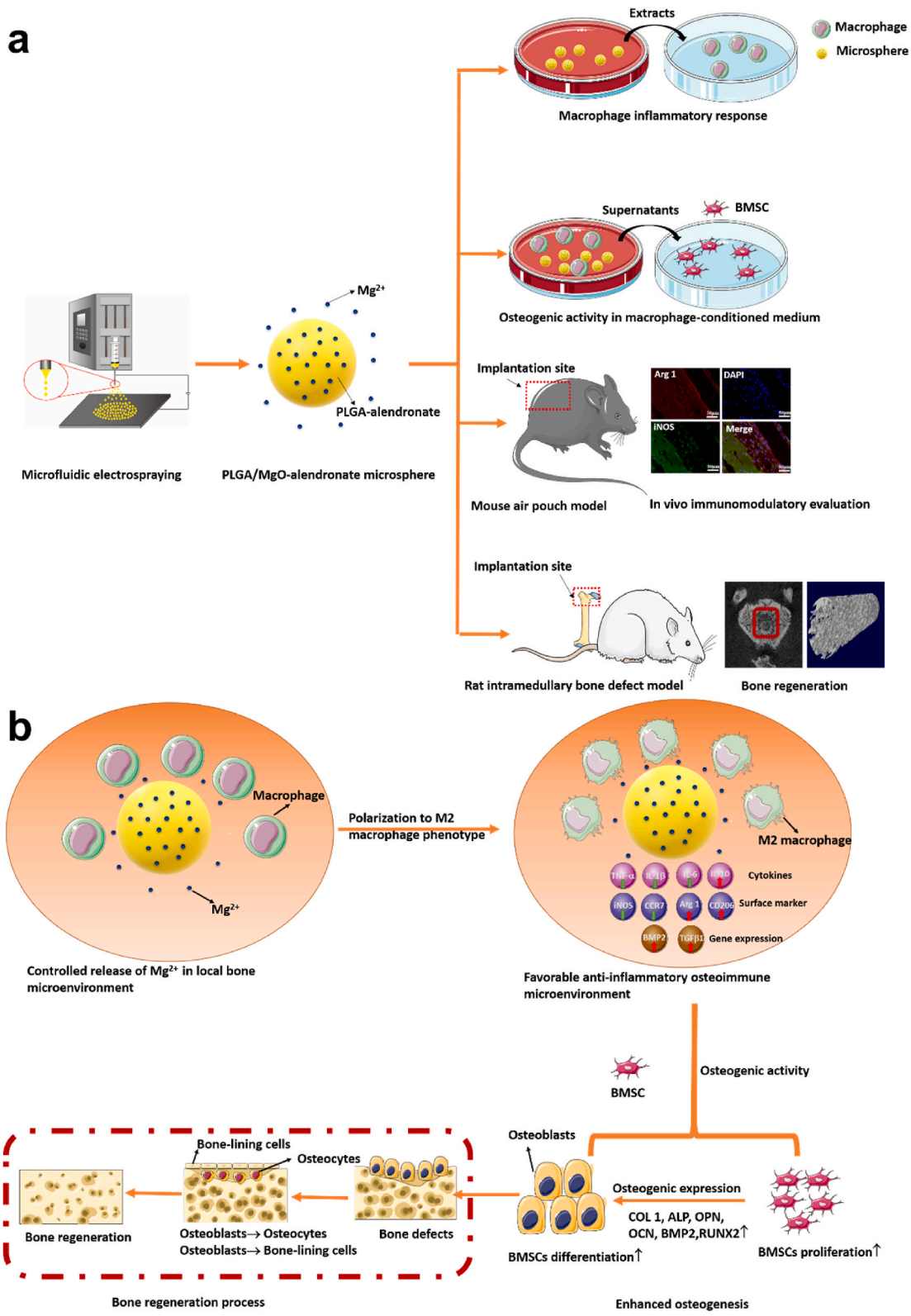

Scheme 1. Schematic illustrations of (a) the concept of *in situ* immunomodulatory osteogenesis using PLGA/MgO-alendronate microsphere delivery system fabricated by microfluidic electrospraying and (b) proposed mechanism of the osteoimmune environment generated by controlled release of Mg^{2+} to accelerate bone regeneration *in vivo*.

PLGA/MgO microspheres were synthesized under a voltage of 11 kV by the same method.

2.2. Sample characterization

The surface morphology of PLGA-based microspheres was characterized by a scanning electron microscope (SEM, Hitachi S–3400 N,

Japan) at 5 kV. In order to detect the inner microstructure and magnesium distribution of microspheres, samples were cut into cross-sections by a cryostat (Leica) and characterized by SEM. Molecular structures of PLGA-based microspheres were measured by the Fourier-transform infrared (FTIR) transmission spectra at ambient temperature.

2.3. Hydroxyapatite (HA) binding assay

The bone affinity of PLGA-based microspheres was evaluated by the HA binding assay. Briefly, HA nanoparticles (<100 nm, Sigma) were added in Tris/HCl-buffered saline solution (50 mM, pH 7.4) at a concentration of 10 mg/ml 20 mg PLGA-based microspheres were added into 200 μl HA suspension followed by gently shaken for 4 h. Next, the solution was subjected to centrifugation at 10000× g for 10 min. The amount of HA nanoparticles in each group's suspension was determined by the UV/VIS spectrophotometer (UV-1601, Japan) at 337 nm. The rate of HA binding in each group was determined as follow:

HA binding (%) = (1-absorbance (337 nm) of sample suspensions)/ absorbance (337 nm) of HA nanoparticle suspensions ×100.

2.4. Mg^{2+} release profile in vitro

The Mg^{2+} release profiles were measured by immersing a certain amount of PLGA/MgO and PLGA/MgO-alendronate microspheres in PBS (pH 7.4) at 37 °C. Specifically, 10 mg PLGA-based microspheres were immersed in 1 ml PBS for 1, 3, 5, 7, 14, 21, and 28 days and the accumulative release of Mg^{2+} was determined by the inductively-coupled plasma optical emission spectrometry (ICP-OES, Optima 2100DV; USA)., The PBS solution was gently centrifuged, and 600 μl supernatants were collected at each time point, followed by measuring the concentration of magnesium ion through the ICP-OES machine at 37 °C.

2.5. In vitro cytocompatibility

2.5.1. Cell culture

The murine-derived macrophage cells (RAW264.7; ATCC), fibroblasts (3T3), and rat bone marrow mesenchymal stem cells (BMSCs; Cyagen Biosciences Inc; RASMX-01001) were utilized in the *in vitro* experiment. The two cell lines were incubated with the Dulbecco's Modified Eagle's Medium (DMEM) solutions consisting of 10% fetal bovine serum (Gbico, USA), 100 μg ml^{-1} streptomycin, and 100 U ml^{-1} penicillin at 37 °C under humidified conditions with 5% CO_2. Cell passages occurred if cells proliferated to 80–90% confluence. The DMEM solutions were refreshed every two days.

2.5.2. 3T3 fibroblasts proliferation

The CCK-8 assay was used to determine the proliferation of 3T3 fibroblasts incubated with PLGA-based microspheres for 1 and 4 days. Prior to the experiment, PLGA-based microspheres were sterilized by gamma-ray sterilization (30 min). 1×10^4 cells/well 3T3 fibroblasts were seeded on microsphere samples into a 24-well plate at 37 °C. At each time point, a 10% CCK-8 solution containing DMEM was added for another 4 h incubation. Afterward, 100 μl supernatants were aspirated into a 96-well plate, and a micro-plate spectrophotometer (Thermo Scientific, USA) was employed to determine the absorbance at 450 nm. The OD values on day 4 were normalized to those of day 1 to calculate the relative proliferation rate of 3T3 fibroblasts.

2.5.3. RAW cell polarization

The *in vitro* polarization of macrophages (RAW264.7) was qualitatively evaluated by immunofluorescence staining assays by monitoring the expression levels of inducible nitric oxide synthase (iNOS) and Arginase 1 (Arg 1). The extracts of PLGA-based microspheres were prepared by immersing 0.1 g/ml microspheres into the DMEM solution at 37 °C for 72 h according to the standard of ISO10993. Briefly, 1×10^5 cells/well RAW264.7 were incubated with extracts of PLGA-based microspheres into a 12-well plate for 4 days. Then, the RAW cells were fixed by 4% paraformaldehyde for 15 min) and blocked by 1% bovine serum albumin (BSA; 1 h) solutions. All of the three solutions were purchased from Sigma (USA). The cells were incubated with primary antibodies iNOS (1:50; Novus Biologicals) and Arg 1 (1:50; Abcam) at 4 °C overnight, followed by the addition of secondary antibodies donkey anti-rabbit Alexa Fluor 488 (1:200; Abcam) and donkey anti-mouse Alexa Fluor 594 (1:200; Abcam) for further incubation (2 h) at ambient temperature. Subsequently, the DAPI solution was used to stain the nuclei for 5 min, and a fluorescence microscope obtained the morphology of RAW264.7. The control group was defined as RAW cells incubated without extracts of microspheres at the same conditions.

The ratio of M1 and M2 macrophages (RAW 264.7) incubated with extracts of PLGA-based microspheres was determined by flow cytometry analysis via analyses of the expressions of the cluster of differentiation 206 (CD206 marker) and C–C motif chemokine receptor type 7 (CCR7, M1 marker). All the antibodies were purchased from eBioscience (USA). 1×10^5 cells/well RAW cells were seeded on a 12-well plate at 37 °C. After incubation for 4 days, RAW cells were centrifuged and rinsed with 1% BSA for 0.5 h to block non-specific antigens. The phycoerythrin (PE)-conjugated CD206 and allophycocyanin (APC)-conjugated CCR7 were employed to stain RAW cells at room temperature for 1 h; concurrently, the isotype controls were composed of APC-conjugated rat IgG2a,κ, PE-conjugated rat IgG2a,κ, and FITC-conjugated rat IgG2a,κ. The cells were rinsed with 1% BSA three times and 100 μl suspensions aspirated into a new 96-well plate for analysis through a flow cytometer (Thermo Fisher Scientific, USA).

2.5.4. Cytokine secretion and gene expression of RAW cells

Inflammatory cytokines secreted by RAW264.7 were examined by the enzyme-linked immunosorbent kits (ELISA, R&D Systems; USA). Similar to the aforementioned incubation condition, the culture DMEM were centrifuged for 4 days, and the supernatants were used to measure the level of tumor necrosis factor-α (TNF-α), interleukin (IL)-1β, IL-6, and IL-10 following the ELISA kit's instructions. The gene expressions were characterized by the RT-PCR assay. Specifically, 5×10^5 cells/well RAW264.7 cells were incubated with extracts of PLGA-based microspheres on a 6-well plate for 4 days. The extracts containing 10% FBS were refreshed every 2 days, and a Trizol reagent (Invitrogen, USA) was applied for RNA extraction following the kit's instructions. A NanoDrop 1000 spectrophotometer (Thermo Scientific, USA) was utilized to detect the total RNA concentration. The total quantitative PCR reaction system included 5 μl primers (listed in Table S1, Supplementary Information), 5 μl cDNA template, and 10 μl SYBR Green PCR Master Mix (Applied Biosystems, USA); the Bio-Rad Thermal Cycler machine was utilized to detect the expression of iNOS, Arg1, TGF-β1 and BMP-2. The reacted signal was amplified by setting 39 cycles.

2.5.5. Osteogenic activity of BMSCs in macrophage-conditioned medium

Prior to the experiments, the cell attachment was performed to determine the cytotoxicity of samples on BMSCs. BMSCs (1×10^4 cells/well) were incubated with PLGA-based microspheres into a 24-well plate at 37 °C for 24 h. BMSCs were washed by PBS three times and then dehydrated using an ethanol solution (50%, 70%, 80%, 90%, and 100%) for 10–15 min, respectively. Finally, samples were subjected to critical point drying equipped with liquid CO_2 for 48 h, and the morphology of BMSCs was obtained by a SEM at 5 kV.

The macrophage-conditioned medium was prepared by incubating RAW 264.7 cells on microsphere samples for 4 days, collecting the supernatants, and mixing them with fresh DMEM at a ratio of 1:1. The CCK-8 assay described in Section2.5.2 was conducted to measure the cell viability of BMSCs on the macrophage-conditioned medium for 1 and 3 days. The 5-Bromo-2′-deoxyUridine (BrdU) incorporation assay was applied to evaluate BMSCs' proliferation on days 1 and 3 via an ELISA BrdU kit (Roche, USA). Based on the manufacturer's instruction, a

micro-plate spectrophotometer was used to determine the absorbance at 450 nm and 690 nm (reference).

The alkaline phosphatase (ALP) activity of BMSCs (2×10^4 cells/well) in the macrophage-conditioned medium was measured after incubation for 3, 7, and 14 days. The conditioned medium with the addition of 50 μl ml^{-1} ascorbic acid (Sigma), 10 mM β-glycerol phosphate (Sigma), and 10 nM dexamethasone (Sigma) was refreshed every 2 days. At the prescribed time, BMSCs in a 24-well plate were washed with PBS, lysed, and centrifugated at 4 °C for 10 min. Following this, an ALP reagents kit (Stanbio, USA) was applied to determine each group's ALP activity. The absorbance per minute was measured at 405 nm, and the total protein level was determined via a Bio-Rad Protein Assay. The alizarin red staining (ARS) assay was performed to characterize the mineralization of BMSCs after 21 days of incubation. Calcium deposits were dissolved using 10% cetylpyridinium chloride, and the absorbance at 570 nm was detected. In addition, the RT-PCR assay was also employed to examine the osteogenic expression level of BMSCs (5×10^4 cells/well) incubated with the conditioned medium into a 6-well plate for 7 and 14 days. Similar methods described in section 2.5.4 were applied to detect osteogenic expressions such as ALP, BMP-2, osteopontin (OPN), type collagen I (Col I), runt-related transcription factor 2 (Runx2), and osteocalcin (OCN).

2.6. In vivo animal experiments

The surgical procedures were licensed by the Ethics Committee of the University of Hong Kong, whilst post-operative care protocols were fulfilled by the Licensing Office of the Department of Health, Hong Kong Government.

2.6.1. Mouse air pouch model

Twenty mice (C57BL/6, 8 weeks old) were evenly divided into four groups and employed to investigate *in vivo* immunomodulatory effects of PLGA-based microspheres by establishing an air pouch model. Five mice from each group were used for immunofluorescence, hematoxylin-eosin (HE), and immunohistochemistry staining. The mice were anesthetized by 1% pentobarbital (50 mg/kg) via intraperitoneal injection, and 3 ml sterile air was injected into the dorsal area. Secondary injection of sterile air at the same volume was conducted after 4 days. One day after the secondary injection, a surgical incision was made in the middle of the pouch by injecting 100 mg sterilized PLGA-based microspheres. The air pouch without injection of samples was set as the control group. All the aseptic surgical procedures were followed. All the mice were sacrificed 4 days post-operation.

For *in vivo* immunofluorescence staining, the tissue was harvested from the skin containing the pouch, and PLGA-based microspheres were thoroughly removed from the pouches. Then, the tissue was fixed by 4% paraformaldehyde for 0.5 h. Non-specific antigens of macrophages were blocked by 1% BSA. In order to determine the expression level of surface macrophage markers for M1 (iNOS) and M2 (Arg 1), primary and secondary antibodies were utilized, and the same procedures described in Section 2.5.3 were followed. Immunofluorescence images were observed by a fluorescence microscope.

For histological analysis, the tissue was fixed using 10% buffer formalin solution, embedded in paraffin, and sectioned into 5 μm thick slices. The slices were processed for HE and immunohistochemistry staining to investigate the inflammatory response and percentage of different macrophage phenotype in the fibrous layer. Primary antibodies of iNOS (Novus Biologicals, 1:50) and Arg 1 (Abcam, 1:50) were incubated overnight at 4 °C. Subsequently, the sections were processed with undiluted horseradish peroxidase (HRP)-conjugated secondary antibodies and stained using a diaminobenzidine (DAB) substrate. The nuclei were stained with hematoxylin in the HE analysis and DAPI in the immunohistochemistry analysis. The morphological observation was conducted by a light microscope and fluorescence microscope (Sony DKSST5, Japan). Image-Pro Plus software was applied in analyzing the thickness of the fibrous layer and the ratio of iNOS-positive/Arg 1-positive areas.

2.6.2. Rat intramedullary bone defect model

Twenty-eight Sprague-Dawley (SD) female rats (12 weeks old, female, Laboratory Animal Unit) were utilized to evaluate the bone regeneration capacity induced by PLGA-based microspheres. Seven rats from each group were utilized in the intramedullary bone defect model, and all seven samples were used for micro-CT and histological analyses. The rats were anesthetized by 67 mg/kg ketamine and 6 mg/kg xylazine via intraperitoneal injection. Prior to the surgery, hair shaving and disinfection were performed. The manual driller (diameter: 2 mm) was used to drill through the intramedullary marrow cavity with an injection of sterilized PLGA-based microspheres (0.1 g/ml, mixed with 0.9% saline). The intramedullary bone defect was developed randomly on the right/left femur of rats, as shown in Fig. S1, Supplementary Information. After suturing, Terramycin (1 mg/kg) and ketoprofen (0.5 kg/mg) were subcutaneously injected. All the rats were sacrificed 8 weeks post-surgery. The bone defect without injection of PLGA-based microspheres was defined as the sham control.

The microcomputed tomography machine (micro-CT, SKYSCAN 1076) was used to real-timely monitor bone volume of each group at post-surgery 0, 1, 2, 4, and 8 weeks. At the prescribed time points, the rats were anesthetized and scanned via the micro-CT machine to analyze the bone volume, bone mineral density (BMD), trabecular thickness (Tb, Th), and trabecular number (Tb,N) via the Skyscan Company Software. The grey threshold ranged from −1000 to 9240 in the Hounsfield units. The Giemsa staining was applied for histological analysis of new bone tissue, and the procedures were described in previous work [27]. The Young's moduli of Giemsa-stained slide was determined by a nano-indentation machine. The applied maximum load, drift rate, and peak holding time were set as 10 mN, 1.2 nm S^{-1}, and 120 s.

2.7. Statistical analysis

Five specimens at each time point were included in *in vitro* cell studies performed in triplicate independently. The SPSS v15 software was employed to measure the statistical difference between groups. The experimental data were analyzed using the one-way ANOVA with Tukey's post hoc tests. The p-value of less than 0.05 was considered significantly different.

3. Results

3.1. Characterizations of PLGA-based microspheres

The surface morphology and size distribution of PLGA-based microspheres manufactured by microfluidic electrospraying are presented in Fig. 1a and b. The surface and inner structure of each group with narrow size distribution exhibited pores due to solvent evaporation. Elemental Mg within the microspheres was evenly distributed due to the surface modification of magnesium nanoparticles by TMSPM-coupling modification. Furthermore, the mean diameter of monodisperse PLGA/MgO-alendronate microspheres was 5.5 μm that was slightly higher than that of PLGA and PLGA/MgO microspheres (diameter: 1.6 μm and 1.8 μm, respectively). In order to demonstrate the molecular structure of PLGA-based microspheres, results of FIIR spectra are depicted in Fig. 1c. For the PLGA microspheres group, the absorption peaks at 1048 cm^{-1} and 1455 cm^{-1} were the C–CH_3 stretching vibrations and C–H stretching vibrations in methyl groups, respectively. The peaks at 1085 cm^{-1} and 1755 cm^{-1} referred to C–O–C stretching and C═O stretching vibrations in the ester group. The PLGA/MgO microspheres group exhibited similar FTIR spectra with the PLGA microspheres group. With regards to PLGA/MgO-alendronate microsphere group, the absorption peak at 1640 cm^{-1} was the C═O stretching vibrations of the amide bond in the PLGA-alendronate conjugate, while

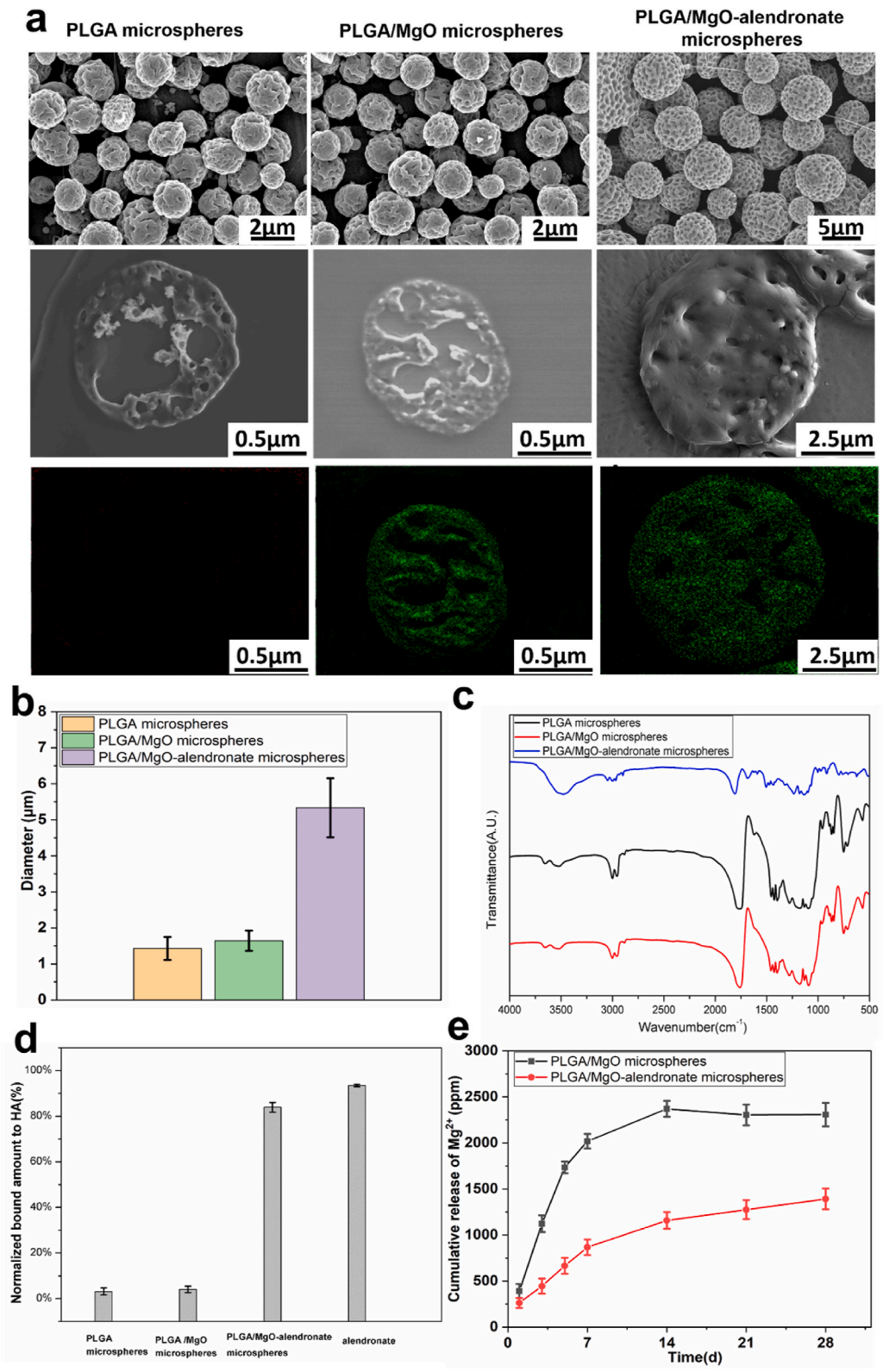

Fig. 1. Characterizations of PLGA-based microspheres fabricated by microfluidic electrospraying. (a) The morphology, inner structure, and Mg element (green) distribution observed by SEM at 5 kV. (b) The size distribution. (c) FTIR spectra (d) The bone affinity property of PLGA-based microspheres evaluated by binding rate to hydroxyapatite (HA) nanoparticles at 37 °C. (e) The accumulative Mg^{2+} release profiles *in vitro* at 37 °C. (For interpretation of the references to colour in this figure legend, the reader is referred to the Web version of this article.)

the peak at 3530 cm^{-1} was due to N–H stretching vibrations of the amide bond, confirming the existence of the amide bond on the PLGA-alendronate microspheres. Since the amide bond was formed by the reaction between the carboxyl group in the PLGA polymer and the amino group in the alendronate, it demonstrated that alendronate was successfully conjugated to the PLGA/MgO microsphere.

Besides, the bone affinity property of PLGA-based microspheres was characterized by the HA binding test in PBS at 37 °C (Fig. 1d). Specifically, the control group's HA binding rate (alendronate) was 95.3%, demonstrating an excellent bone affinity towards hydroxyapatite nanoparticles. The PLGA/MgO-alendronate group exhibited to be higher affinity (approximately 83.9%) for HA nanoparticles due to the conjugation of alendronate than that of PLGA microspheres (3.5%) and PLGA/MgO microspheres (4.1%) respectively, which indicated that

PLGA/MgO-alendronate microspheres showed superior the bone targeting capability. Fig. 1e depicts the magnesium ion release profiles of each group *in vitro*. The PLGA/MgO microsphere group showed a near-order burst release pattern during the first 5 days, followed by a parabolic release pattern until day 28. Furthermore, the near-order burst release rate of the PLGA/MgO group was about 350 ppm/day; the total concentration of 2480 ppm was observed on day 14, implying complete delivery of Mg^{2+} from the PLGA/MgO microsphere within 2 weeks. In contrast, the PLGA/MgO-alendronate microsphere exhibited a release rate of about 120 ppm/day at the first week, whilst a total concentration of Mg^{2+} was less approximately 1200 ppm than that of the PLGA/MgO group during the 4 weeks. More importantly, the controlled release of Mg^{2+} at 50–200 ppm/day could be achieved by the PLGA/MgO-alendronate microsphere for four weeks. Combined with the HA binding rate results in Fig. 1d, it was expected that the PLGA/MgO-alendronate microspheres could achieve bone targeting of the local tissue microenvironment and manipulate the release of magnesium ions, inducing a magnesium-controlled tissue microenvironment (Mg TME) for bone regeneration *in vivo*.

3.2. In vitro biocompatibility of PLGA/MgO-alendronate microspheres

3.2.1. Fibroblasts proliferation

In order to characterize the cytocompatibility of PLGA-based microspheres, the fibroblasts (3T3 cells) proliferation on samples was evaluated by the CCK-8 assay on days 1 and 4 (Fig. 2a). The results revealed that after four days incubation, relative proliferation rate of all the groups exhibited elevation. Furthermore, the relative proliferations of 3T3 cells on PLGA/MgO and PLGA/MgO-alendronate groups at day 4 were statistically 57.4% ($p < 0.01$) and 64.8% ($p < 0.01$) higher than that of the PLGA group, respectively. The CCK-8 results revealed that magnesium ion delivery from microspheres was beneficial to the proliferation of 3T3 fibroblasts and exhibited satisfactory cytocompatibility *in vitro*.

3.2.2. Polarization, inflammatory response, and osteogenic gene expressions of RAW cells

Immunofluorescence staining and flow cytometry were employed to evaluate the effects of magnesium ions' delivery on the M1/M2 polarization profile of RAW cells, as shown in Fig. 2b–f. Fig. 2b displays the images of representative markers (iNOS, M1, green) and (Arg1, M2, red) RAW264.7 cells cultured for 4 days. RAW cells on the PLGA/MgO-alendronate microsphere group expressed less iNOS (M1, green) and more Arg 1 (M2, red) compared to the PLGA and PLGA/MgO groups, illustrating that controllable release of magnesium ions induced the macrophage switch to M2 phenotype. To determine the proportion of M1/M2 macrophages, we employed flow cytometry to measure the percentage of the surface markers CCR7-positive (M1 macrophage phenotype) and CD206-positive (M2 macrophage phenotype) RAW cells simultaneously, as shown in Fig. 2c–e. In brief, the results reported that the CCR7 surface marker on RAW264.7 cells cultured with the extracts of PLGA/MgO-alendronate microspheres exhibited 21.63% positive ($p < 0.05$). In contrast, the PLGA/MgO group and PLGA group presented 32.83% and 36.37%, respectively. In contrast, the CD206 positive cells on the PLGA/MgO-alendronate group (43.23%) were significantly higher than that of PLGA (26.03%) and PLGA/MgO (34.83%) samples, respectively. Therefore, the PLGA/MgO-alendronate group induced more M2 phenotype and less M1 phenotype, representing the highest proportion of M2/M1 macrophages.

Fig. 2f–i depicts the concentration of inflammatory cytokines (TNF-α, IL-1β, IL-6, and IL-10) secreted by RAW cells of each group incubation for 4 days. It is apparent that the concentration of pro-inflammatory cytokine TNF-α on the PLGA/MgO-alendronate group (351 pg/ml) showed 36.1% ($p < 0.01$) and 31.2% ($p < 0.01$) decrease in comparison with the PLGA and PLGA/MgO groups. The concentration of IL-6 on the PLGA microsphere group was significantly higher ($p < 0.05$) than that of PLGA/MgO and PLGA/MgO-alendronate groups. The lower concentration of IL-1β was also detected on the PLGA/MgO-alendronate group compared to the PLGA group. In contrast, IL-10 secreted on the PLGA/MgO-alendronate group exhibited 60.4% ($p < 0.05$) and 45.5% ($p < 0.05$) increase. Additionally, gene expressions of iNOS, Arg 1, BMP-2, and TGF-β1 were measured by the RT-PCR assay (Fig. 2j–m). Expression of M1 surface marker gene iNOS was down-regulated on the PLGA/MgO-alendronate group, whereas up-regulation of M1 surface marker gene Arg 1 was observed. Furthermore, the up-regulation of BMP-2 and TGF-β1 on the PLGA/MgO-alendronate group exhibited 123.1% ($p < 0.05$) and 47.2% ($p < 0.05$) increase. All these results demonstrated that RAW cells cultured on the PLGA/MgO-alendronate group secreted enhanced levels of anti-inflammatory cytokines and decreased levels of pro-inflammatory cytokines to facilitate polarization to M2 macrophage phenotype.

3.2.3. Osteogenic activity of BMSCs in macrophage-conditioned medium

In order to investigate the immunomodulatory effects of PLGA-based microspheres on osteogenesis, the osteogenic capability of BMSCs was evaluated in a macrophage-conditioned medium. Fig. 3a depicts the morphology of BMSCs seeded on PLGA-based microspheres for 24 h. The cells were flattened, and more BMSCs adhered to the microspheres containing MgO nanoparticles. All the groups presented favorable BMSCs adhesion, indicating the non-toxicity of PLGA-based microspheres towards BMSCs. Then, BMSCs were incubated with the macrophage-conditioned medium to determine the osteogenic activity. In terms of viability, proliferation, osteogenic differentiation, and mineralization of BMSCs (Fig. 3b–f), the results of the CCK-8 assay showed that the PLGA/MgO and PLGA/MgO-alendronate microsphere groups exhibited elevated cell viability of BMSCs due to the magnesium ion delivery. The PLGA/MgO-alendronate group's cell viability was statistically 19% ($p < 0.01$) higher than that of the PLGA group on day 3. The BrdU incorporation assay revealed enhanced proliferation of the PLGA/MgO microsphere group on day 1. Moreover, the fold change of BMSCs proliferation on PLGA/MgO-alendronate microsphere groups showed a significant two and half times ($p < 0.001$) increase on day 3, indicating that the release of Mg^{2+} was beneficial for the proliferation of BMSCs. The differentiation of BMSCs was evaluated by the ALP activity of BMSCs seeded on the conditioned medium in each group for 3, 7, and 14 days. On day 3, relatively low ALP activity and no obvious difference were observed among all the groups since BMSCs were still at the proliferation stage. When cultured for 7 and 14 days, the ALP expression of PLGA/MgO-alendronate group presented 34.7% ($p < 0.05$) and 44.7% ($p < 0.05$) increase, respectively. Furthermore, the ALP activity was even statistically 55.1% ($p < 0.05$) and 83.3% ($p < 0.05$) higher than the PLGA/MgO microsphere group on days 7 and 14. Additionally, alizarin red absorbance on the PLGA/MgO-alendronate microsphere group exhibited 50.6% ($p < 0.01$) and 58.2% ($p < 0.01$) increase after 21 days incubation. It was implied that the osteoimmune environment induced by PLGA/MgO-alendronate microsphere was favorable to the differentiation and mineralization of BMSCs.

With respect to osteogenic expressions, we examined the osteogenic expressions of ALP, OPN, Col I, Runx2, OCN, and BMP-2 in BMSCs incubated with the macrophage-conditioned medium for 7 and 14 days, as presented in Fig. 3g–k. Specifically, on day 7, the Col I expression of the PLGA/MgO-alendronate group was 71.4% ($p < 0.05$) and 50.2% ($p < 0.05$) higher than that of PLGA and PLGA/MgO groups, respectively, while the OPN and OCN expressions were up-regulated 61.1% ($p < 0.05$) and 55.6% ($p < 0.05$). When cultured for 14 days, the OCN and ALP expressions showed an approximately 1.5-fold ($p < 0.05$) and one-fold ($p < 0.05$) increase. Remarkably elevated expressions of Col I, BMP-2, Runx2, and OPN ($p < 0.05$) were also observed, implying that controllable release of Mg^{2+} from PLGA/MgO-alendronate microsphere was more conducive to osteogenic-related gene expressions *in vitro*.

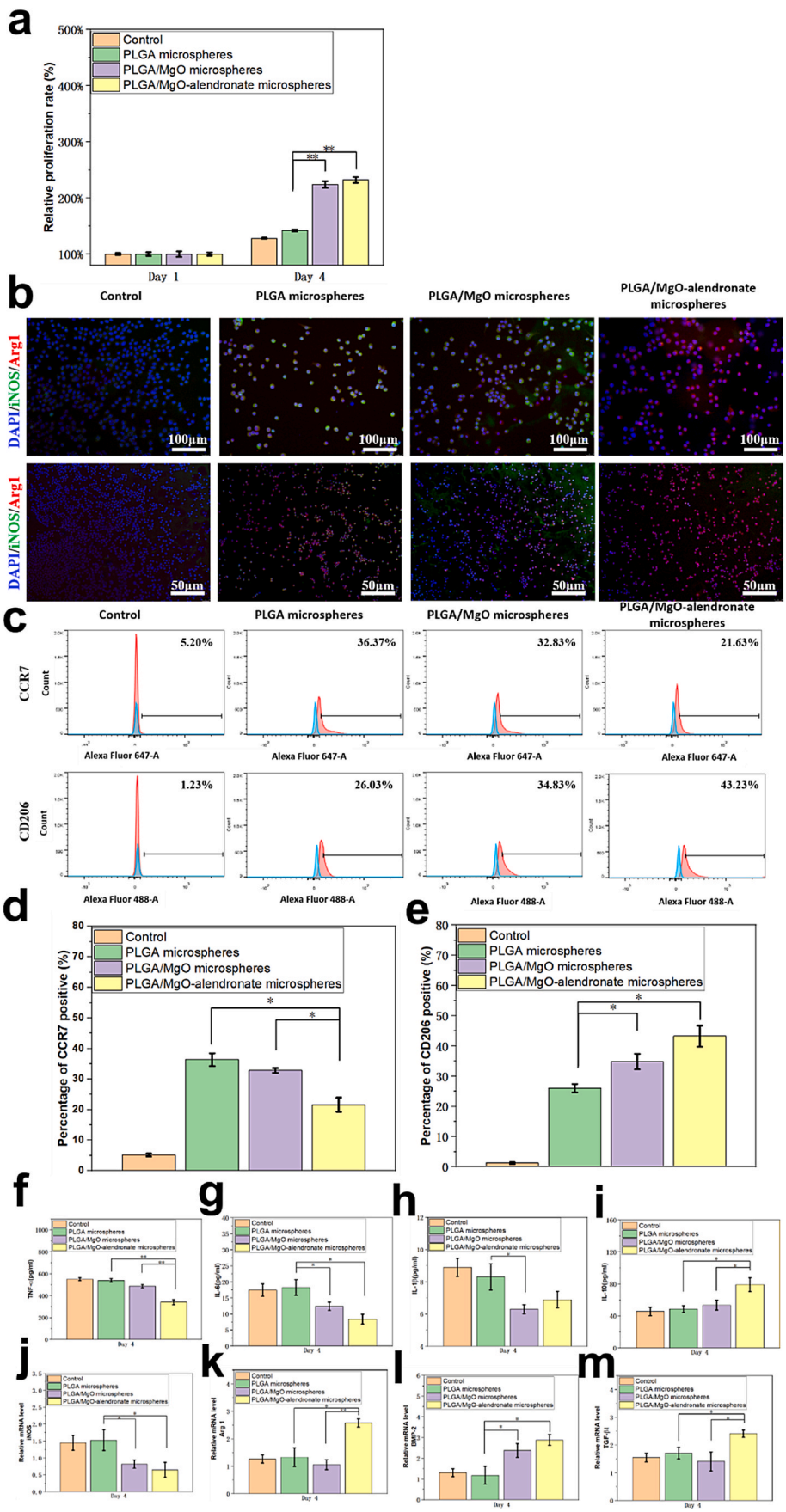

Fig. 2. The 3T3 fibroblasts proliferation, polarization, cytokine secretion, and relative mRNA expression levels of RAW264.7 cells incubated with the extracts of PLGA-based microspheres at 37 °C for 4 days. (a) The 3T3 fibroblasts' proliferation on each group characterized by the CCK-8 assay for 1 and 4 days at 37 °C. (b) The immunofluorescent images of RAW cells in each group and (c)–(e) the flow cytometry results of surface markers (CCR7 and CD206) of polarized RAW cells. It was obvious that the increased proportion of the M2 phenotype and decreased ratio of the M1 phenotype were observed on the PLGA/MgO-alendronate microsphere group. (f)–(i) The cytokine productions of TNF-α, IL-6, IL-1β and IL-10 secreted by RAW cells measured by ELISA kits and (j)–(m) the relative mRNA expressions of macrophage surface markers (iNOS, Arg 1) and osteogenic growth factors (BMP-2, TGF-β1) normalized to GAGDH. The control group was denoted as macrophages incubated in the normal DMEM. * represented the significantly difference ($p < 0.05$); ** ($p < 0.01$). (surface marker iNOS, CCR7: green, M1 phenotype; surface marker Arg 1, CD206: red, M2 phenotype; DAPI: blue, nuclei). (For interpretation of the references to colour in this figure legend, the reader is referred to the Web version of this article.)

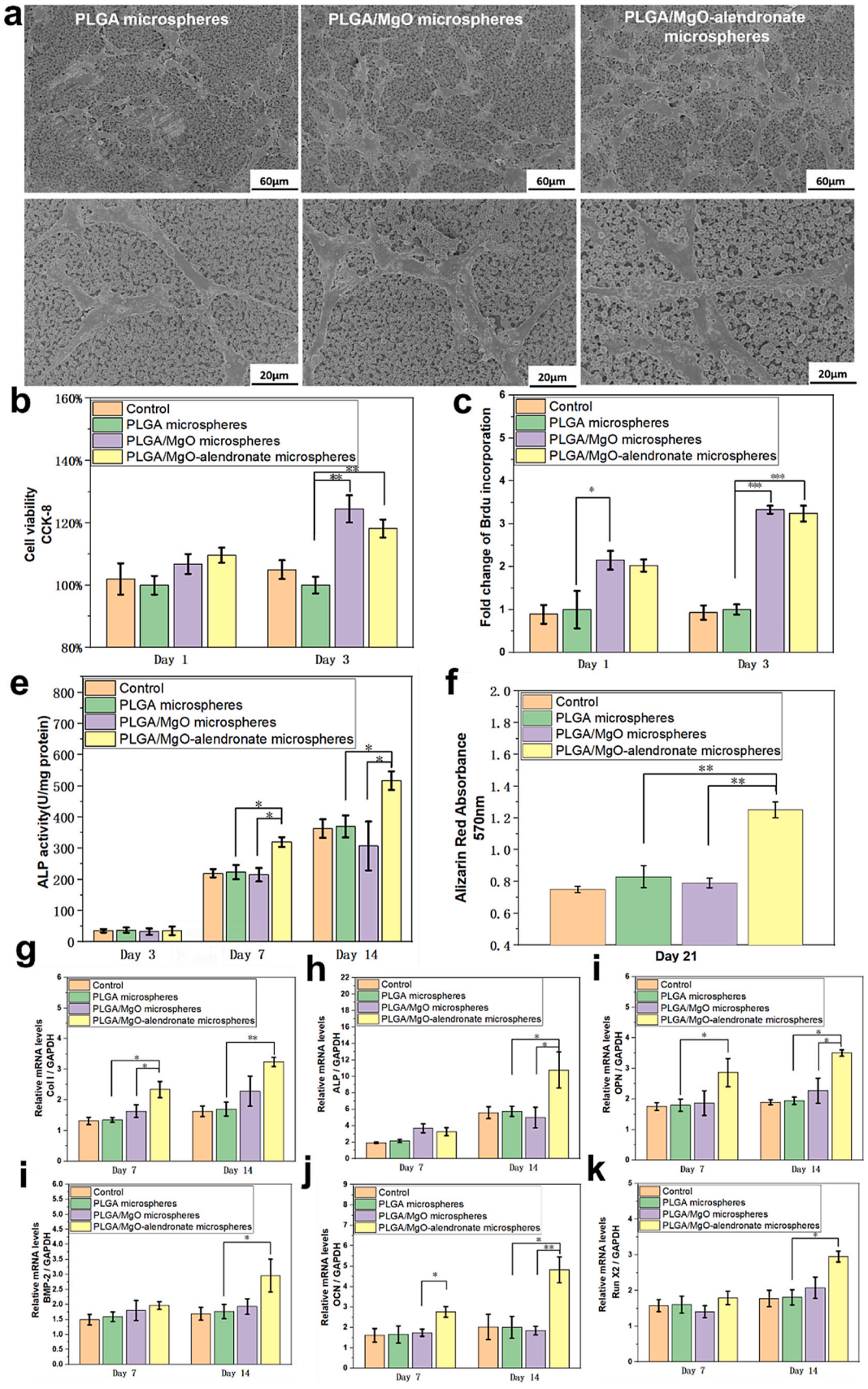

(caption on next page)

Fig. 3. The osteogenesis of BMSCs cultured in macrophage-conditioned medium. The medium was prepared by incubating RAW cells with PLGA-based microspheres at 37 °C for 4 days and then aspirating the culture's supernatants. (a) The morphology of BMSCs seeded on PLGA-based microspheres for 24 h observed by SEM to evaluate surface morphology. The BMSCs attached well and even flattened on PLGA/MgO-alendronate microsphere. (b)–(f) The cell viability, proliferation, differentiation, and mineralization of BMSCs incubated with macrophage-conditioned medium at various time points. The cell viability and proliferation were analyzed by CCK-8 and BrdU incorporation assay, while the ALP activity and alizarin red tests were employed to determine osteogenic differentiation and mineralization of BMSCs. (g)–(k) The relative mRNA osteogenic levels of Col 1, ALP, OPN, OCN, BMP-2, and Runx2 of BMSCs normalized to GAPDH detected by the RT-PCR assay on days 7 and 14. The control group was defined as BMSCs cultured in DMEM without the addition of PLGA-based microspheres. * referred to a significant difference ($p < 0.05$); ** ($p < 0.01$); *** ($p < 0.001$). (For interpretation of the references to colour in this figure legend, the reader is referred to the Web version of this article.)

3.3. *In vivo* animal studies

3.3.1. *Results of the mouse air pouch model*

We performed *in vivo* immunomodulatory evaluations for inflammatory levels, various phenotypes of macrophages, immunofluorescence staining, HE, and immunohistochemistry histological analysis on a mouse air pouch model. Fig. 4a displays the immunofluorescence and HE histological images of the skin sections for each group 4 days post-surgery. Among all the groups, the PLGA/MgO-alendronate microsphere group exhibited the highest M2 macrophages (Arg 1, red) and lowest M1 macrophages (iNOS, green), according to the immunofluorescence images. The fibrous layer's thickness remarkably reduced compared with the PLGA group, indicating a milder inflammatory reaction. The statistical results (Fig. 4a) consistently shows that the PLGA/MgO-alendronate group's fibrous layer thickness was 76.9% ($p < 0.05$) lower than that of the PLGA group. The ratio of $iNOS^+/Arg^+$ 1 in the PLGA/MgO group was slightly higher than that of the PLGA group. Moreover, the ratio of $iNOS^+/Arg^+$ 1 on the PLGA/MgO-alendronate group was 71.5% lower ($p < 0.05$) than that of PLGA/MgO and PLGA groups in immunofluorescence staining.

As depicted in Fig. 4b, the trend of Arg 1 expression was as follows: PLGA/MgO-alendronate group > PLGA group > PLGA/MgO group in the immunohistochemistry images. In contrast, the lowest iNOS expression was observed in the PLGA/MgO-alendronate group. Similarly, as compared with the PLGA and PLGA/MgO groups, the ratio of $iNOS^+/Arg^+$ 1 of PLGA/MgO-alendronate group remarkably reduced,

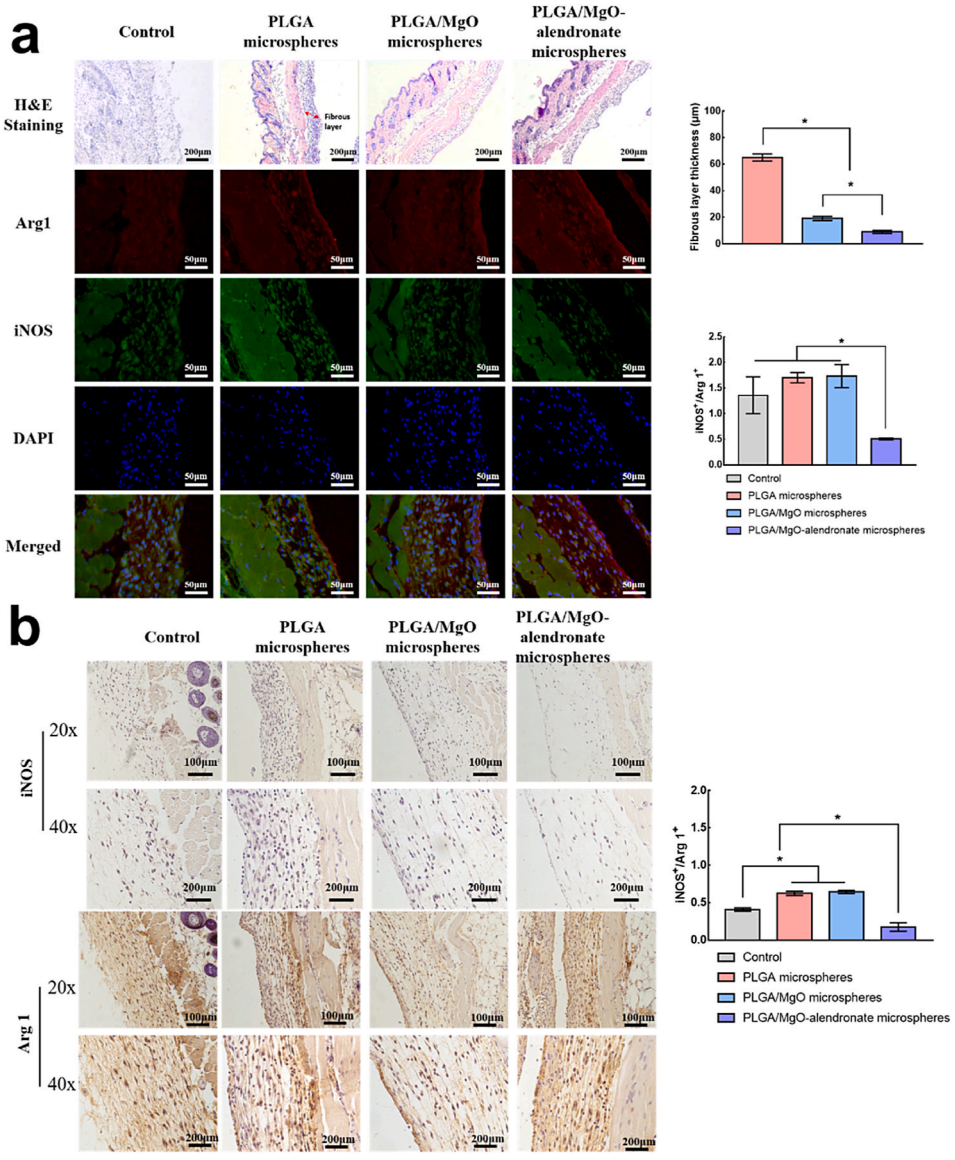

Fig. 4. The *in vivo* immunomodulatory evaluations of PLGA-based microspheres in the mouse air pouch model. (a) The quantitive and qualitative of surface markers iNOS (green, M1 phenotype) and Arg 1 (red, M2 phenotype) expressions by immunofluorescence analysis and hematoxylin-eosin (HE) analysis on the sectioned skin tissue 4 days post-surgery. The thickness of the fibrous layer, the percentage of iNOS-positive and Arg 1-positive cells were quantitatively analyzed by the Image-Pro Plus software. (b) The qualitative immunohistochemistry analysis and quantitative analysis of iNOS- and Arg 1-positive areas by the Image-Pro Plus software in sectioned skin tissues 4 days post-operation. * referred to a significant difference ($p < 0.05$). (For interpretation of the references to colour in this figure legend, the reader is referred to the Web version of this article.)

implying that Mg controlled osteoimmune environment induced by the PLGA/MgO-alendronate group promoted M2 macrophage phenotype and reduced M1 phenotype *in vivo*. Based on these results, PLGA/MgO-alendronate microsphere could trigger an M2 macrophage switch and a favorable anti-inflammatory local microenvironment.

3.3.2. Results of rat intramedullary bone defect model

A rat intramedullary bone defect model was performed to evaluate bone formation *in vivo*. Fig. 5a depicts the real-time micro-CT images and reconstructed 3D models of new bone tissue at post-operation 0, 1, 2, 4, and 8 weeks. The new bony tissue of the PLGA/MgO and PLGA/MgO-alendronate groups began to form only at post-operation one week. Contrarily, new bone tissue was rarely observed within the sham control and PLGA microsphere group. Moreover, it was evident that bone tissue on the PLGA/MgO-alendronate group was continuously formed along with the implantation time. The defect was almost healed in the reconstructed 3D model 8 weeks post-surgery. For the PLGA/MgO microsphere group, the bone volume was far less than that of the PLGA/MgO-alendronate group, although new bony tissue was gradually observed at the same post-operation time. In contrast, both the PLGA microsphere and sham control groups exhibited a low degree of bone formation in reconstructed 3D models. To quantitatively analyze the newly-formed bony tissue, we employed the Skyscan Software to calculate the percentage of new bone volume, Tb,Th, BMD, and Tb,N at various time points, portrayed in Fig. 5b. In comparison with the control and PLGA groups, the percentage of bone volume on the PLGA/MgO-alendronate group was statistically higher ($p < 0.01$) on post-operation two weeks, and the bone volume even exhibited about 2.5-fold increase ($p < 0.001$) on week 4 and 8. Furthermore, a remarkably higher percentage of new bone volume was observed at week 4 ($p < 0.01$) and 8 ($p < 0.001$) compared with the PLGA/MgO microsphere group, respectively. In addition, the BMD and Tb,Th were even 33.3% ($p < 0.05$) and 21.4% ($p < 0.05$) higher than that of the PLGA/MgO group on post-surgery eight weeks.

Fig. 5c reveals histological images stained by the Giemsa solution and Young's moduli of new bone tissue on post-operation eight weeks. The bone defect of the PLGA/MgO-alendronate group was remarkably filled with plenty of bony tissue. In contrast, the sham, PLGA, and PLGA/MgO microsphere groups displayed a relatively slow bone healing process with bone defects on the rats' femur. Moreover, the new cancellous bone with well-mineralized structures was formed within the defects on the PLGA/MgO-alendronate group. Additionally, Young's moduli of new bony tissue on the PLGA/MgO-alendronate group exhibited to be 11.8 GPa at week 8, which was statistically 38.8% ($p < 0.05$), 47.9% ($p < 0.05$), and 29.7% ($p < 0.05$) higher than that of shame control, PLGA and PLGA/MgO microsphere groups respectively. These results suggested that the PLGA/MgO-alendronate microsphere could induce bone formation with the comparable mechanical property.

4. Discussion

The development of bone substitutes for bone repair or regeneration usually involves the direct activation of osteoprogenitor cells for osteogenesis. However, the cross-talk between the skeletal system and the immune system during the bone healing process has frequently been overlooked. The homeostasis of immune cells significantly impacts bone remodeling and regeneration [28,29]. Prior to osteogenesis and angiogenesis, the early inflammatory reaction of immune cells to the biomaterial surface mainly determines the fate of implantation *in vivo* [30]. The physicochemical properties of biomaterials via modulating the plasticity of macrophages in cellular polarization can, in turn, be utilized to regulate the associated immunological reactions to maintain a balance between osteoimmunomodulation and osteointegration at the vicinity of implants [31]. Hence, it seems to be the new strategy for designing next-generation orthopedic substitutes by developing biomaterials with an osteoimmunomodulatory function to promote osteogenesis and, subsequently, generate a suitable osteoimmune microenvironment. Recently, stimulation of bone formation by magnesium ions released from biomaterials (e.g., metallic implant, bio-polymer, and bio-ceramic) has drawn much attention owing to the high efficacy, low cost, and reduced complication [32–35]. The delivery of magnesium ions at a suitable range of concentrations contributes to osteogenesis by promoting osteoblastic activity and inhibiting osteoclastic activity and facilitating the bone mineralization process [36]. However, high doses of magnesium are detrimental to osteoblast differentiation, disruption of the mineralization process, and may even evoke hypermagnesemia clinically through systemic administration [37,38]. Therefore, the local release of magnesium ions in a controllable manner becomes paramount for stimulating new bone formation. Furthermore, previous studies investigated the immunomodulatory effects of Mg^{2+} on osteogenesis. Lima et al. reported that mesenchymal stem cells (MSCs), incubated at culture media with 5 mM Mg^{2+}, could promote the proliferation and modulation of immune responses by enhancing the secretion of anti-inflammatory cytokines (IL-10 and PGE2) and decreasing levels of pro-inflammatory cytokines (IL-6 and IL-1β) [39]. Li et al. reported that magnesium ions delivered from magnesium-doped titanium implants could elevate anti-inflammatory cytokines secreted by M2 macrophages and up-regulate the expression of VEGF and BMP-2 for osteogenesis [18]. Moreover, magnesium-doped calcium phosphate cement (CPC) was capable of modulating macrophage polarization towards osteogenesis and angiogenesis [40]. However, these studies were unable to identify the correlations between Mg^{2+} in bone tissue microenvironments and *in-situ* osteogenesis *in vivo*. The literature rarely emphasizes the relationship between osteoimmune environment regulated by Mg^{2+} and its ability to induce bone regeneration effects *in vivo*.

Our study aims to investigate the osteoimmune effects of Mg^{2+} in bone tissue microenvironments toward *in-situ* bone regeneration using the rat intramedullary defect model. Our newly designed PLGA/MgO-alendronate microsphere enables controlled delivery of Mg^{2+} in the local tissue microenvironment (TME). This new delivery system, with excellent bone binding affinity, is able to adhere to the surface of mineralized bone structure and then modulate the delivery of magnesium ions to local TME utilizing alendronate conjugation [41]. Moreover, the mechanism of controlled delivery of Mg^{2+} from PLGA/MgO-alendronate microsphere was based on alendronate conjugation. Alendronate serves as a kind of bisphosphonates. Zhang et al. developed a nanocomposite hydrogel stabilized by bisphosphonate (BP)–Mg^{2+} to coordinate the sustained release of magnesium ions and subsequent bone formation [42,43]. They reported that two phosphonate -$PO(OH)_2$ groups of bisphosphonate covalently linked to the central carbon atom possessed excellent binding efficiency to various metallic ions (e.g., Mg^{2+}, Cu^{2+}, Ca^{2+}, and Fe^{3+}). As such, the release of these metallic ions could be manipulated. Additionally, it was reported that the alendronate might activate the BMP-related signaling pathway so as to improve the osteogenic differentiation of MSCs [44–46]. Therefore, alendronate alone may be conducive to the osteogenic activity of BMSCs to a certain extent. The *in vitro* and *in vivo* results demonstrate that the PLGA/MgO-alendronate microsphere can generate a favorable anti-inflammatory osteoimmune environment that modulates pro-osteogenic macrophage polarization, thereby facilitating the differentiation of BMSCs and subsequent bone healing *in vivo*.

4.1. Inflammatory response and osteogenic activity of macrophages and BMSCs in magnesium tissue microenvironment in vitro

In order to examine the inflammatory response of macrophages to the exposure of the magnesium tissue microenvironment (Mg TME), we performed *in vitro* experiments to identify the polarization, cytokine secretion, and gene expression of macrophages. Indeed, among a multiple of immune cells, macrophages are one of the most important cells in regulating innate immune response and tissue remodeling through

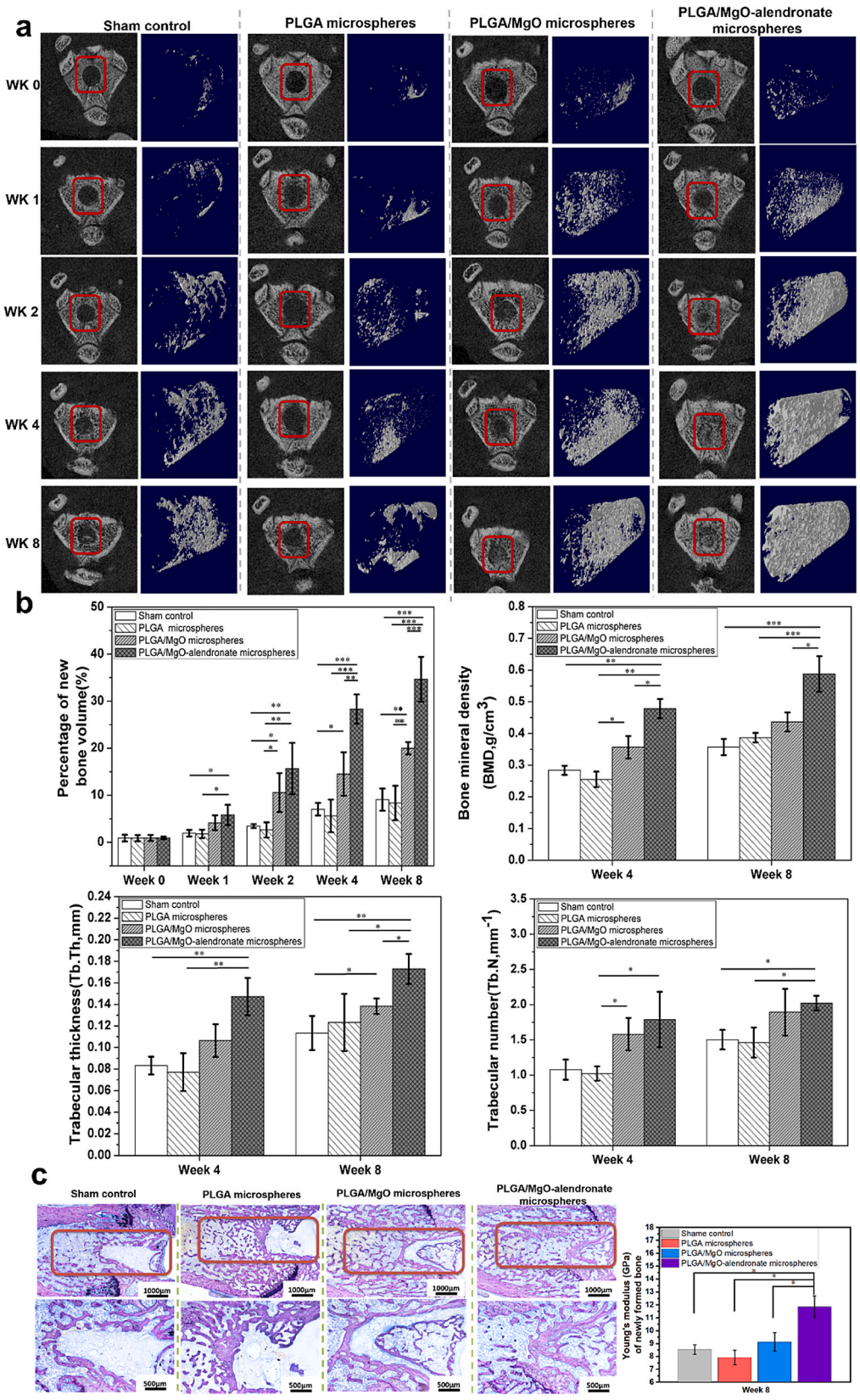

Fig. 5. The bone regeneration of PLGA-based microspheres characterized by using the rat intramedullary bone defect model. (a) The real-time micro-CT analysis and 3D reconstructed u-CT images of new bone formation at post-operation 0, 1, 2, 4, and 8 weeks (the bone defect highlighted by the red box). (b) The percentage of new bone volume, BMD, Tb,Th, and Tb.N of bone tissue. (c) The histological analysis of each group stained by the Giemsa solutions and Young's modulus of new bone formation measured by the nano-indentation machine after post-surgery eight weeks. * defined as a significant difference ($p < 0.05$); ** ($p < 0.01$); *** ($p < 0.001$). (For interpretation of the references to colour in this figure legend, the reader is referred to the Web version of this article.)

the secretion of inflammatory cytokines that recruit other immune cells to commit to the battlefield (implant site). Moreover, macrophages can easily switch to other phenotypes to respond to the surrounding tissue microenvironment stimuli, which favors tissue regeneration [10,47,48]. The immunofluorescence results in Fig. 2b clearly reveals that the controlled magnesium TME (PLGA/MgO-alendronate microsphere group) up-regulated Arg 1 (M2 surface marker) expression and down-regulated iNOS (M1 surface marker) expression, indicating that a majority of macrophages actively polarized to the M2 phenotype. Furthermore, the flow cytometry results quantitively presented the higher proportion of M2 phenotype and smaller fraction of M1 on the controlled magnesium TME, implying that the controlled Mg TME is more conducive to reduce M1 phenotype polarization. Moreover, magnesium can suppress the production of pro-inflammatory cytokines via inhibited activation of NF-kB and TLR pathways, leading to low M1 phenotype switch [49–51]. In order to address the critical concentration of Mg^{2+} on macrophage phenotype switch, Lima et al. systematically investigated the effects of magnesium (0, 1, 3, and 5 mM) on immunomodulatory properties of MSCs [39]. Magnesium ions at the concentration of 5 mM (120 ppm) could elevate the proliferation of MSCs, while M1 to M2 macrophage phenotype polarization also occurred. In our *in vitro* results, the PLGA/MgO-alendronate microsphere maintained the release of Mg^{2+} at 50–200 ppm for the first 3 days, which significantly activated the macrophage phenotype switch from M1 to M2, enhancing the osteogenic differentiation of BMSCs. Hence, we hypothesized that the critical dose of extracellular magnesium on macrophage phenotype switch should be at ~100–200 ppm. However, the exact concertation of Mg^{2+} used requires further investigations.

The cytokine levels analyzed by ELISA further confirmed the immunomodulatory property of controlled Mg TME on macrophage polarization. The RAW cells on the PLGA/MgO-alendronate group secreted a higher concentration of anti-inflammatory cytokine (IL-10) and reduced the expressions of pro-inflammatory cytokines (TNF-α, IL-6, and IL-1β). TNF-α and IL-1β suppressed osteoblastic differentiation, synthesis of alkaline phosphate by osteoblasts, and mineralization of the extracellular bone matrix (ECM), while IL-6 accelerated osteoclastogenesis and osteoclastic functions via the activation of receptor activator of NF-kB ligand (RANKL) [52–54]. The anti-inflammatory cytokine IL-10, secreted by M2 phenotype, elevated the differentiation of osteoblasts [55]. In terms of gene expression, enhanced expression of Arg 1 (M2 surface marker) and decreased expression of iNOS (M1 surface marker) were observed in this study. Additionally, two osteogenic-related expressions (BMP-2 and TGF-β1) were significantly up-regulated by controlled Mg TME, which plays a pivotal role in osteogenesis and bone healing. TGF-β, recognized as upstream of the BMP signaling pathway, is also a crucial osteogenic factor, triggering the osteogenic differentiation of MSCs into osteoblasts [56]. BMP-2 and TGF-β1, which are two well-known signaling molecules of the TGF-β superfamily, can stimulate osteogenesis and angiogenesis through the BMP-2R and TGF-β1R receptors [57,58].

The literatures propose that a quick macrophage switch from M1 to M2 phenotype at an initial stage of bone injury was helpful to the recruitment of MSCs to the implantation site and therefore enhance osteoblastic differentiation [21,59,60]. Thus, we evaluated the osteogenic capability of BSMCs when cultured in the conditioned osteoimmune microenvironment (Fig. 3). The cell viability and proliferation of BMSCs were elevated in the macrophage-conditioned medium of the PLGA/MgO-alendronate group. Also, the differentiation and mineralization of BSMCs were significantly promoted. The up-regulation of osteogenic expressions could be attributed to the osteoimmune tissue microenvironment modulated by controlled Mg delivery. It is believed that the aforementioned BMP-2 and TGF-β1 bind to their respective receptors, BMP-2R and TGF-β1R, which activate the transcription of osteogenic-related genes, e.g., Runx2, OCN, ALP, and Col 1 via the potentiating BMP2 signaling pathway [61–64]. Hence, the increased expressions of BMP-2 and TGF-β1 in the osteoimmune tissue microenvironment may contribute to enhanced osteoblastic differentiation. Moreover, the beneficial effects of Mg^{2+} release on MSCs proliferation and differentiation have been verified by a previous study [65]. However, it seems that the optimal concentration of Mg^{2+} for MSCs proliferation and differentiation is still controversial. Glesske et al. revealed that Mg^{2+}, at a concentration of 2.5–10 mM, could maintain human BMSCs viability, proliferation, and differentiation [66]. However, the mineralized matrix deposition and differentiation of BMSCs were inhibited when exposed to magnesium ion concentrations higher than 1.3 mM [67].

In this study, we aim to identify the osteoimmune effect of the Mg^{2+}-enriched bone tissue microenvironment. Based on the results of this study and our previous studies, we believe that Mg^{2+} release and the osteoimmune tissue microenvironment decorated by PLGA/MgO-alendronate microspheres can synergistically contribute to the promoted differentiation of BMSCs. The PLGA/MgO-alendronate microspheres generate an anti-inflammatory osteoimmune tissue microenvironment that triggers the macrophage switch from M0 to M2 phenotype. Then, the secretion of anti-inflammatory cytokines may elevate the differentiation of BMSCs. However, we are unable to exclude the direct contribution of Mg^{2+} delivery on the osteogenic differentiation of bone marrow mesenchymal stem cells (BMSCs).

4.2. Immunomodulatory evaluation and bone regeneration in vivo

Although our *in vitro* experiments demonstrate how macrophages coordinate bone regeneration in the osteoimmunomodulatory tissue microenvironment mediated by magnesium ions, this observation becomes less convincing without the proof by *in vivo* animal study. Thus, we further investigated the *in vivo* immunomodulatory effects in controlled Mg TME using the mouse pouch air model. The pouch air model has been widely utilized to study various types of inflammation due to the advantages of high sensitivity and convenience for histological analysis [68]. When biomaterials are implanted, macrophages are recruited to the biomaterial surface and attempt to coalesce with foreign body giant cells (FBGCs), which is associated with the formation of the fibrous capsule on biomaterials. The thickness of the fibrous layer is highly correlated to the degree of innate inflammation *in vivo*. The results in Fig. 4a show that the thickness of the fibrous layer on the controlled Mg TME (PLGA/MgO-alendronate microsphere group) significantly decreased in comparison to other groups, suggesting that the suppression of foreign body reaction and modulation of macrophages switch to M2 phenotype at an early stage of inflammation could be observed. Furthermore, the immunofluorescence and immunohistochemistry results (Fig. 4b) further confirm that controlled Mg TME (PLGA/MgO-alendronate microsphere) could induce a higher proportion of Arg1 positive cells (M2 macrophages) and a lower ratio of iNOS positive cells (M1 macrophages) at the injury site, indicating that the elevated M2/M1 ratio and favorable anti-inflammatory, immune microenvironment were achieved.

In order to observe the osteoimmune-mediated bone regeneration *in vivo*, a rat intramedullary defect model was employed to assess the bone regeneration effects. A large amount of newly formed bony tissue 2 weeks post-operation was observed on the controlled Mg TME (PLGA/MgO-alendronate group) in 3D reconstructed models by micro-CT scans (Fig. 5). The bone defect was almost completely healed 8 weeks post-surgery; moreover, the enhanced BMD, Tb.Th and Tb,N of new bone tissue on the PLGA/MgO-alendronate group, were obtained. Most importantly, the enhanced Young's moduli and mineralized bone structure could also be observed in the controlled Mg TME group, implying that the newly formed bone's mechanical property was superior. With respect to the *in vivo* results, the PLGA/MgO-alendronate microspheres induced a large amount of bone formation at an early stage and accelerated the bone healing process. However, the PLGA/MgO-alendronate microspheres could not be applied alone to deal with the critical-size bone defect, as the microspheres are unable to

provide any mechanical support to the defect. Hence, it is suggested that the microspheres may incorporate with other bone scaffolds or fillers, e.g., 3D printed scaffolds and PMMA cements, in order to establish a magnesium-enriched local tissue microenvironment for *in-situ* bone regeneration.

All these results indicate that controlled Mg TME modulates the milder anti-inflammatory microenvironment, thereby facilitating subsequent bone regeneration. To be specific, bone regeneration derived from the macrophages-mediated inflammatory response is affected by a smooth switch of macrophages from pro-inflammatory M1 to anti-inflammatory M2 phenotype at the early stage of implantation (3–4 days) [11]. Herein, the macrophage switch to M2 phenotype accompanied by the secretion of anti-inflammatory cytokines on the PLGA/MgO-alendronate microsphere group induces a favorable immune microenvironment towards osteoimmunomodulation. In addition, the slightly elevated pH caused by the controlled release of Mg^{2+} was also conducive to improved osteogenesis and bone formation [69,70]. In contrast, both of the control groups (PLGA and PLGA/MgO microsphere) exhibited a smaller amount of new bone formation 2 weeks post-operation due to the high ratio of the M1 phenotype and elevated pro-inflammatory cytokines (TNF-α and IL-6) production in the bone tissue microenvironment. The persistence of the M1 phenotype and the failure of the M2 phenotype switches may have caused the local tissue inflammation that resulted in poor bone formation [71]. Furthermore, the PLGA/MgO microsphere presented a burst release of magnesium ions that generated an excessive magnesium-enriched microenvironment in bony tissue. This adverse TME may have jeopardized the proliferation and osteogenic differentiation of BMSCs and disorganized the bone mineralization process, leading to compromised new bone formation in terms of bone volume, bone mineral density (BMD), trabecular bone thickness and number (Tb.Th), and its Young's moduli [72,73].

In summation, Scheme 1b proposes the osteoimmunomodulatory functions of the PLGA/MgO-alendronate microsphere delivery system. With the help of alendronate conjugation, the delivery system is able to decorate the bone tissue microenvironment with an appropriate amount of magnesium ions at the initial stage of implantation. The immune cells, typically macrophages, are recruited to the injury site and then initiate an immune response upon arrival. The macrophages then polarize into the M2 phenotype that secretes a high level of IL-10 and a decreased level of TNF-α, IL-6 and IL-1β cytokines. The up-regulated osteogenic expressions of BMP-2 and TGF-β1 by macrophages are also obtained. Therefore, a mild inflammatory response generates a favorable anti-inflammatory osteoimmune microenvironment, stimulating osteogenic cell recruitment. The BMSCs are then recruited to the injury site, and the proliferation of BMSCs also occurs due to the controlled Mg TME. The BMSCs tend to osteogenic differentiation with the enhanced expressions of ALP, Col 1, OPN, OCN, BMP-2, and Runx2. These genes are actively involved in promoting osteogenesis, accelerating mineralization, and the bone regeneration process.

5. Conclusion

The osteoimmunomodulatory effects of controlled magnesium bone tissue microenvironment (Mg TME) on macrophage polarization and subsequent bone regeneration can be achieved by a customized PLGA/MgO-alendronate microsphere delivery system. The controlled Mg TME is able to induce M2 phenotype macrophage switch accompanied by a high level of IL-10 cytokine secretion and enhanced osteogenic expression of BMP-2 and TGF-β1. In addition, the cytokines, including TNF-α, IL-6 and IL-1β have been remarkably suppressed. This favorable anti-inflammatory and pro-osteogenic tissue microenvironment can then promote the proliferation and differentiation of BMSCs via upregulation of ALP, OCN, OPN, Col 1, Runx2, and BMP-2 and, therefore, accelerate subsequent bone regeneration *in vivo*. The newly formed bone tissues in the Mg TME possess a superior microstructure, bone mineral density, and mechanical property. Hence, we believe that this *in situ* immunomodulatory osteogenesis approach can be realized using the PLGA/MgO-alendronate microsphere delivery system.

Author contributions

Z.Lin performed the experiments and wrote the manuscript. K.W.K. Yeung and Z.Lin conceived the experiments and interpreted the data. D. Shen and W.Zhou performed the *in vitro* macrophage study and *in vivo* inflammatory evaluations. Y.F.Zheng, T.T.Kong and X.L.Liu interpreted the *in vitro* data while S.L.Wu, K.M.C.Cheung and J.Wu interpreted the results of *in vivo* rat bone defect model. Paul K. Chu and Y.Zhao contributed the magnesium ion release curves.

CRediT authorship contribution statement

Zhengjie Lin: Writing - original draft, Conceptualization, Methodology. **Danni Shen:** Methodology, Investigation. **Weixiao Zhou:** Methodology, Investigation. **Yufeng Zheng:** Formal analysis. **Tiantian Kong:** Formal analysis, Visualization. **Xuanyong Liu:** Formal analysis. **Shuilin Wu:** Formal analysis. **Paul K. Chu:** Formal analysis. **Ying Zhao:** Formal analysis. **Jun Wu:** Formal analysis. **Kenneth M.C. Cheung:** Supervision. **Kelvin W.K. Yeung:** Conceptualization, Supervision.

Declaration of competing interest

The authors declare that they have no known competing financial interests or personal relationships that could have appeared to influence the work reported in this paper.

Acknowledgement

The authors gratefully acknowledge Ms. Lv Minmin (Core Lab, The University of Hong Kong-Shenzhen Hospital) for explaining the Flow cytometry data. This work was financially supported by the National key R&D Program of China (2018YFC1105100), Guangdong Basic and Applied Basic Research Foundation (2019A1515111156), China Postdoctoral Science Foundation (2019M653060), NSFC/RGC Joint Research Scheme (No. N_HKU725/16), Health and Medical Research Fund (19180712), Shenzhen Science and Technology Funds (JSGG20180507183242702), Hong Kong Innovation Technology Fund (ITS/287/17 and ITS/405/18), Hong Kong Research Grant Council General Research Fund (No. 17214516), the Science and Technology Commission of Shanghai Municipality (No. 18410760600), International Partnership Program of Chinese Academy of Sciences (GJHZ1850) and National Natural Science Foundation of China (81572113).

Appendix A. Supplementary data

Supplementary data to this article can be found online at https://doi.org/10.1016/j.bioactmat.2021.01.018.

References

[1] V. Campana, G. Milano, E. Pagano, M. Barba, C. Cicione, G. Salonna, et al., Bone substitutes in orthopaedic surgery: from basic science to clinical practice, J. Mater. Sci. Mater. Med. 25 (2014) 2445–2461.
[2] D.C. Lobb, B.R. DeGeorge Jr., A.B. Chhabra, Bone graft substitutes: current concepts and future expectations, J. Hand Surg. 44 (2019) 497–505. e2.
[3] Z. Chen, J. Yuen, R. Crawford, J. Chang, C. Wu, Y. Xiao, The effect of osteoimmunomodulation on the osteogenic effects of cobalt incorporated β-tricalcium phosphate, Biomaterials 61 (2015) 126–138.
[4] Z. Sheikh, N. Hamdan, Y. Ikeda, M. Grynpas, B. Ganss, M. Glogauer, Natural graft tissues and synthetic biomaterials for periodontal and alveolar bone reconstructive applications: a review, Biomater. Res. 21 (2017) 9.
[5] G. Zhou, T. Groth, Host responses to biomaterials and anti-inflammatory design—a brief review, Macromol. Biosci. 18 (2018), 1800112.

[6] R. Trindade, T. Albrektsson, P. Tengvall, A. Wennerberg, Foreign body reaction to biomaterials: on mechanisms for buildup and breakdown of osseointegration, Clin. Implant Dent. Relat. Res. 18 (2016) 192–203.
[7] Y. Li, Y. Xiao, C. Liu, The horizon of materiobiology: a perspective on material-guided cell behaviors and tissue engineering, Chem. Rev. 117 (2017) 4376–4421.
[8] A. Vishwakarma, N.S. Bhise, M.B. Evangelista, J. Rouwkema, M.R. Dokmeci, A. M. Ghaemmaghami, et al., Engineering immunomodulatory biomaterials to tune the inflammatory response, Trends Biotechnol. 34 (2016) 470–482.
[9] K.L. Spiller, S. Nassiri, C.E. Witherel, R.R. Anfang, J. Ng, K.R. Nakazawa, et al., Sequential delivery of immunomodulatory cytokines to facilitate the M1-to-M2 transition of macrophages and enhance vascularization of bone scaffolds, Biomaterials 37 (2015) 194–207.
[10] R. Sridharan, A.R. Cameron, D.J. Kelly, C.J. Kearney, F.J. O'Brien, Biomaterial based modulation of macrophage polarization: a review and suggested design principles, Mater. Today 18 (2015) 313–325.
[11] J. Lee, H. Byun, S.K. Madhurakkat Perikamana, S. Lee, H. Shin, Current advances in immunomodulatory biomaterials for bone regeneration, Adv. Healthcare Mater. 8 (2019) 1801106.
[12] A. Mantovani, S.K. Biswas, M.R. Galdiero, A. Sica, M. Locati, Macrophage plasticity and polarization in tissue repair and remodelling, J. Pathol. 229 (2013) 176–185.
[13] Z. Chen, X. Mao, L. Tan, T. Friis, C. Wu, R. Crawford, et al., Osteoimmunomodulatory properties of magnesium scaffolds coated with β-tricalcium phosphate, Biomaterials 35 (2014) 8553–8565.
[14] L. Bai, Z. Du, J. Du, W. Yao, J. Zhang, Z. Weng, et al., A multifaceted coating on titanium dictates osteoimmunomodulation and osteo/angio-genesis towards ameliorative osseointegration, Biomaterials 162 (2018) 154–169.
[15] J.M. Sadowska, F. Wei, J. Guo, J. Guillem-Marti, M.-P. Ginebra, Y. Xiao, Effect of nano-structural properties of biomimetic hydroxyapatite on osteoimmunomodulation, Biomaterials 181 (2018) 318–332.
[16] L. Mao, L. Xia, J. Chang, J. Liu, L. Jiang, C. Wu, et al., The synergistic effects of Sr and Si bioactive ions on osteogenesis, osteoclastogenesis and angiogenesis for osteoporotic bone regeneration, Acta Biomater. 61 (2017) 217–232.
[17] W. Zhang, C. Feng, G. Yang, G. Li, X. Ding, S. Wang, et al., 3D-printed scaffolds with synergistic effect of hollow-pipe structure and bioactive ions for vascularized bone regeneration, Biomaterials 135 (2017) 85–95.
[18] B. Li, H. Cao, Y. Zhao, M. Cheng, H. Qin, T. Cheng, et al., In vitro and in vivo responses of macrophages to magnesium-doped titanium, Sci. Rep. 7 (2017) 42707.
[19] C. Schmitz, A.-L. Perraud, Magnesium and the immune response. Molecular, Genetic, and Nutritional Aspects of Major and Trace Minerals, Elsevier, 2017, pp. 319–331.
[20] A. Shahi, S. Aslani, M. Ataollahi, M. Mahmoudi, The role of magnesium in different inflammatory diseases, Inflammopharmacology (2019) 1–13.
[21] B. Li, P. Gao, H. Zhang, Z. Guo, Y. Zheng, Y. Han, Osteoimmunomodulation, osseointegration, and in vivo mechanical integrity of pure Mg coated with HA nanorod/pore-sealed MgO bilayer, Biomater. Sci. 6 (2018) 3202–3218.
[22] J.F. Navarro-González, C. Mora-Fernández, J. García-Pérez, Reviews: clinical implications of disordered magnesium homeostasis in chronic renal failure and dialysis. Seminars in Dialysis, Wiley Online Library, 2009, pp. 37–44.
[23] M. Leidi, F. Dellera, M. Mariotti, J.A. Maier, High magnesium inhibits human osteoblast differentiation in vitro, Magnes. Res. 24 (2011) 1–6.
[24] Z. Lin, J. Wu, W. Qiao, Y. Zhao, K.H. Wong, P.K. Chu, et al., Precisely controlled delivery of magnesium ions thru sponge-like monodisperse PLGA/nano-MgO-alginate core-shell microsphere device to enable in-situ bone regeneration, Biomaterials 174 (2018) 1–16.
[25] E.H. Nafea, M.A. El-Massik, L.K. El-Khordagui, M.K. Marei, N.M. Khalafallah, Alendronate PLGA microspheres with high loading efficiency for dental applications, J. Microencapsul. 24 (2007) 525–538.
[26] E. Cenni, D. Granchi, S. Avnet, C. Fotia, M. Salerno, D. Micieli, et al., Biocompatibility of poly (D, L-lactide-co-glycolide) nanoparticles conjugated with alendronate, Biomaterials 29 (2008) 1400–1411.
[27] H.M. Wong, S. Wu, P.K. Chu, S.H. Cheng, K.D. Luk, K.M. Cheung, et al., Low-modulus Mg/PCL hybrid bone substitute for osteoporotic fracture fixation, Biomaterials 34 (2013) 7016–7032.
[28] C. Schlundt, H. Schell, S.B. Goodman, G. Vunjak-Novakovic, G.N. Duda, K. Schmidt-Bleek, Immune modulation as a therapeutic strategy in bone regeneration, J. Exp. Orthop. 2 (2015) 1–10.
[29] G. Mori, P. D'Amelio, R. Faccio, G. Brunetti, The interplay between the bone and the immune system, Clin. Dev. Immunol. 2013 (2013).
[30] S. Franz, S. Rammelt, D. Scharnweber, J.C. Simon, Immune responses to implants–a review of the implications for the design of immunomodulatory biomaterials, Biomaterials 32 (2011) 6692–6709.
[31] R.J. Schutte, A. Parisi-Amon, W.M. Reichert, Cytokine profiling using monocytes/macrophages cultured on common biomaterials with a range of surface chemistries, J. Biomed. Mater. Res. Part A: An Official Journal of The Society for Biomaterials 88 (2009) 128–139. The Japanese Society for Biomaterials, and The Australian Society for Biomaterials and the Korean Society for Biomaterials.
[32] H.M. Wong, K.W. Yeung, K.O. Lam, V. Tam, P.K. Chu, K.D. Luk, et al., A biodegradable polymer-based coating to control the performance of magnesium alloy orthopaedic implants, Biomaterials 31 (2010) 2084–2096.
[33] H.M. Wong, Y. Zhao, F.K. Leung, T. Xi, Z. Zhang, Y. Zheng, et al., Functionalized polymeric membrane with enhanced mechanical and biological properties to control the degradation of magnesium alloy, Adv. Healthcare Mater. 6 (2017).
[34] Z. Lin, Y. Zhao, P.K. Chu, L. Wang, H. Pan, Y. Zheng, et al., A functionalized TiO2/Mg2TiO4 nano-layer on biodegradable magnesium implant enables superior bone-implant integration and bacterial disinfection, Biomaterials 219 (2019) 119372.
[35] Z. Lin, S. Wu, X. Liu, S. Qian, P.K. Chu, Y. Zheng, et al., A surface-engineered multifunctional TiO2 based nano-layer simultaneously elevates the corrosion resistance, osteoconductivity and antimicrobial property of a magnesium alloy, Acta Biomater. 99 (2019) 495–513.
[36] S. Ding, J. Zhang, Y. Tian, B. Huang, Y. Yuan, C. Liu, Magnesium modification up-regulates the bioactivity of bone morphogenetic protein-2 upon calcium phosphate cement via enhanced BMP receptor recognition and Smad signaling pathway, Colloids Surf. B Biointerfaces 145 (2016) 140–151.
[37] D.G. Haider, G. Lindner, S.S. Ahmad, T. Sauter, M. Wolzt, A.B. Leichtle, et al., Hypermagnesemia is a strong independent risk factor for mortality in critically ill patients: results from a cross-sectional study, Eur. J. Intern. Med. 26 (2015) 504–507.
[38] C. Thongprayoon, W. Cheungpasitporn, N. Srivali, S. Erickson, Admission serum magnesium levels and the risk of acute respiratory failure, Int. J. Clin. Pract. 69 (2015) 1303–1308.
[39] F. da Silva Lima, A.B. da Rocha Romero, A. Hastreiter, A. Nogueira-Pedro, E. Makiyama, C. Colli, et al., An insight into the role of magnesium in the immunomodulatory properties of mesenchymal stem cells, J. Nutr. Biochem. 55 (2018) 200–208.
[40] M. Wang, Y. Yu, K. Dai, Z. Ma, Y. Liu, J. Wang, et al., Improved osteogenesis and angiogenesis of magnesium-doped calcium phosphate cement via macrophage immunomodulation, Biomater. Sci. 4 (2016) 1574–1583.
[41] T. Sato, M. Ebara, S. Tanaka, T.-A. Asoh, A. Kikuchi, T. Aoyagi, Rapid self-healable poly (ethylene glycol) hydrogels formed by selective metal–phosphate interactions, Phys. Chem. Chem. Phys. 15 (2013) 10628–10635.
[42] K. Zhang, S. Lin, Q. Feng, C. Dong, Y. Yang, G. Li, et al., Nanocomposite hydrogels stabilized by self-assembled multivalent bisphosphonate-magnesium nanoparticles mediate sustained release of magnesium ion and promote in-situ bone regeneration, Acta Biomater. 64 (2017) 389–400.
[43] K. Zhang, Q. Feng, J. Xu, X. Xu, F. Tian, K.W. Yeung, et al., Self-Assembled injectable nanocomposite hydrogels stabilized by bisphosphonate-magnesium (Mg2+) coordination regulates the differentiation of encapsulated stem cells via dual crosslinking, Adv. Funct. Mater. 27 (2017).
[44] P. Wei, Z. Yuan, W. Jing, Y. Huang, Q. Cai, B. Guan, et al., Strengthening the potential of biomineralized microspheres in enhancing osteogenesis via incorporating alendronate, Chem. Eng. J. 368 (2019) 577–588.
[45] L. Rojo, B. Gharibi, R. McLister, B.J. Meenan, S. Deb, Self-assembled monolayers of alendronate on Ti6Al4V alloy surfaces enhance osteogenesis in mesenchymal stem cells, Sci. Rep. 6 (2016) 30548.
[46] S. Tarafder, S. Bose, Polycaprolactone-Coated 3D printed tricalcium phosphate scaffolds for bone tissue engineering: in vitro alendronate release behavior and local delivery effect on in vivo osteogenesis, ACS Appl. Mater. Interfaces 6 (2014) 9955–9965.
[47] Y. Qie, H. Yuan, C.A. Von Roemeling, Y. Chen, X. Liu, K.D. Shih, et al., Surface modification of nanoparticles enables selective evasion of phagocytic clearance by distinct macrophage phenotypes, Sci. Rep. 6 (2016) 1–11.
[48] C.-H. Lee, Y.-J. Kim, J.-H. Jang, J.-W. Park, Modulating macrophage polarization with divalent cations in nanostructured titanium implant surfaces, Nanotechnology 27 (2016), 085101.
[49] Z. Zhai, X. Qu, H. Li, K. Yang, P. Wan, L. Tan, et al., The effect of metallic magnesium degradation products on osteoclast-induced osteolysis and attenuation of NF-κB and NFATc1 signaling, Biomaterials 35 (2014) 6299–6310.
[50] B. Rochelson, O. Dowling, N. Schwartz, C.N. Metz, Magnesium sulfate suppresses inflammatory responses by human umbilical vein endothelial cells (HuVECs) through the NFκB pathway, J. Reprod. Immunol. 73 (2007) 101–107.
[51] F. Gao, B. Ding, L. Zhou, X. Gao, H. Guo, H. Xu, Magnesium sulfate provides neuroprotection in lipopolysaccharide-activated primary microglia by inhibiting NF-κB pathway, J. Surg. Res. 184 (2013) 944–950.
[52] R.S. Taichman, P.V. Hauschka, Effects of interleukin-1β and tumor necrosis factor-α on osteoblastic expression of osteocalcin and mineralized extracellular matrix in vitro, Inflammation 16 (1992) 587–601.
[53] M.H.A. Meguid, Y.H. Hamad, R.S. Swilam, M.S. Barakat, Relation of interleukin-6 in rheumatoid arthritis patients to systemic bone loss and structural bone damage, Rheumatol. Int. 33 (2013) 697–703.
[54] F. Yoshitake, S. Itoh, H. Narita, K. Ishihara, S. Ebisu, Interleukin-6 directly inhibits osteoclast differentiation by suppressing receptor activator of NF-κB signaling pathways, J. Biol. Chem. 283 (2008) 11535–11540.
[55] Q. Zhang, B. Chen, F. Yan, J. Guo, X. Zhu, S. Ma, et al., Interleukin-10 inhibits bone resorption: a potential therapeutic strategy in periodontitis and other bone loss diseases, BioMed Res. Int. 2014 (2014).
[56] G. Chen, C. Deng, Y.-P. Li, TGF-β and BMP signaling in osteoblast differentiation and bone formation, Int. J. Biol. Sci. 8 (2012) 272.
[57] L.N. Ramoshebi, T.N. Matsaba, J. Teare, L. Renton, J. Patton, U. Ripamonti, Tissue engineering: TGF-[beta] superfamily members and delivery systems in bone regeneration, Expet Rev. Mol. Med. 4 (2002) 1.
[58] M.B. Asparuhova, J. Caballé-Serrano, D. Buser, V. Chappuis, Bone-conditioned medium contributes to initiation and progression of osteogenesis by exhibiting synergistic TGF-β1/BMP-2 activity, Int. J. Oral Sci. 10 (2018) 1–9.
[59] Q.-L. Ma, L.-Z. Zhao, R.-R. Liu, B.-Q. Jin, W. Song, Y. Wang, et al., Improved implant osseointegration of a nanostructured titanium surface via mediation of macrophage polarization, Biomaterials 35 (2014) 9853–9867.
[60] J.A. Jones, D.T. Chang, H. Meyerson, E. Colton, I.K. Kwon, T. Matsuda, et al., Proteomic analysis and quantification of cytokines and chemokines from biomaterial surface-adherent macrophages and foreign body giant cells, J. Biomed. Mater. Res. Part A: An Official Journal of The Society for Biomaterials 83 (2007)

585–596. The Japanese Society for Biomaterials, and The Australian Society for Biomaterials and the Korean Society for Biomaterials.
[61] R. Derynck, Y.E. Zhang, Smad-dependent and Smad-independent pathways in TGF-β family signalling, Nature 425 (2003) 577–584.
[62] J. Wei, J. Shimazu, M.P. Makinistoglu, A. Maurizi, D. Kajimura, H. Zong, et al., Glucose uptake and Runx2 synergize to orchestrate osteoblast differentiation and bone formation, Cell 161 (2015) 1576–1591.
[63] B.A. Byers, A.J. García, Exogenous Runx2 expression enhances in vitro osteoblastic differentiation and mineralization in primary bone marrow stromal cells, Tissue Eng. 10 (2004) 1623–1632.
[64] K. Nakashima, X. Zhou, G. Kunkel, Z. Zhang, J.M. Deng, R.R. Behringer, et al., The novel zinc finger-containing transcription factor osterix is required for osteoblast differentiation and bone formation, Cell 108 (2002) 17–29.
[65] J.M. Díaz-Tocados, C. Herencia, J.M. Martínez-Moreno, A.M. De Oca, M. E. Rodríguez-Ortiz, N. Vergara, et al., Magnesium chloride promotes osteogenesis through notch signaling activation and expansion of mesenchymal stem cells, Sci. Rep. 7 (2017) 7839.
[66] K. Glenske, P. Donkiewicz, A. Köwitsch, N. Milosevic-Oljaca, P. Rider, S. Rofall, et al., Applications of metals for bone regeneration, Int. J. Mol. Sci. 19 (2018) 826.
[67] L. Zhang, C. Yang, J. Li, Y. Zhu, X. Zhang, High extracellular magnesium inhibits mineralized matrix deposition and modulates intracellular calcium signaling in human bone marrow-derived mesenchymal stem cells, Biochem. Biophys. Res. Commun. 450 (2014) 1390–1395.
[68] P.H. Wooley, R. Morren, J. Andary, S. Sud, S.-Y. Yang, L. Mayton, et al., Inflammatory responses to orthopaedic biomaterials in the murine air pouch, Biomaterials 23 (2002) 517–526.
[69] A.L. Bronckers, D.M. Lyaruu, Magnesium, pH regulation and modulation by mouse ameloblasts exposed to fluoride, Bone 94 (2017) 56–64.
[70] D.A. Bushinsky, Metabolic alkalosis decreases bone calcium efflux by suppressing osteoclasts and stimulating osteoblasts, Am. J. Physiol. Ren. Physiol. 271 (1996) F216–F222.
[71] Z. Chen, T. Klein, R.Z. Murray, R. Crawford, J. Chang, C. Wu, et al., Osteoimmunomodulation for the development of advanced bone biomaterials, Mater. Today 19 (2016) 304–321.
[72] R.A. Lindtner, C. Castellani, S. Tangl, G. Zanoni, P. Hausbrandt, E.K. Tschegg, et al., Comparative biomechanical and radiological characterization of osseointegration of a biodegradable magnesium alloy pin and a copolymeric control for osteosynthesis, J. Mech. Behav. Biomed. Mater. 28 (2013) 232–243.
[73] E. Abed, R. Moreau, Importance of melastatin-like transient receptor potential 7 and cations (magnesium, calcium) in human osteoblast-like cell proliferation, Cell Prolif 40 (2007) 849–865.